

Spectral Energy Distributions of a Large Sample of BL Lacertae Objects

E. Nieppola^{*1}, M. Tornikoski² and E. Valtaoja^{1,3}

¹ Tuorla Observatory, Väisäläntie 20, FIN–21500 Piikkiö, Finland

² Metsähovi Radio Observatory, Metsähovintie 114, FIN–02540 Kylmäla, Finland

³ Dept. of Physical Sciences, University of Turku, FIN–20100 Turku, Finland

Received / Accepted

Abstract. We have collected a large amount of multifrequency data for the objects in the Metsähovi Radio Observatory BL Lacertae sample and computed their spectral energy distributions (SED) in the $\log \nu - \log \nu F$ –representation. This is the first time the SEDs of BL Lacs have been studied with a sample of over 300 objects. The synchrotron components of the SEDs were fitted with a parabolic function to determine the synchrotron peak frequency, ν_{peak} . We checked the dependence between luminosities at several frequency bands and synchrotron peak frequency to test the blazar sequence scenario, which states that the source luminosity depends on the location of the synchrotron peak. We also calculated broad band spectral indices and plotted them against each other and ν_{peak} .

The range of ν_{peak} in our study was considerably extended compared to previous studies. There were 22 objects for which $\log \nu_{peak} > 19$. The data shows that at 5 GHz, 37 GHz and 5500 Å there is negative correlation between luminosity and ν_{peak} , whereas in X-rays the correlation turns slightly positive. There is no significant correlation between source luminosity at synchrotron peak and ν_{peak} . Several low radio luminosity–low energy peaked BL Lacs were found. The negative correlation between broad band spectral indices and ν_{peak} is also significant, although there is substantial scatter. Therefore we find that neither α_{rx} nor α_{ro} can be used to determine the synchrotron peak of BL Lacs. On the grounds of our results we conclude that the blazar sequence scenario is not valid. In all our results the BL Lac population is continuous with no hint of the bimodality of the first BL Lac samples.

Key words. galaxies: active – BL Lacertae objects: general – Radiation mechanisms: non-thermal

1. Introduction

BL Lacertae (BL Lacs) are a subclass of active galactic nuclei (AGN). They are characterized by the lack of strong emission lines, rapid variability at all wavelengths and strong polarization. Their spectral energy distribution (SED), in the $\log \nu - \log \nu F$ –representation, consists of a synchrotron component at lower frequencies and an inverse Compton component at higher frequencies. The peculiar traits of the BL Lac class are most likely caused by Doppler–boosted radiation emanating from a relativistic jet aligned close to the line of sight (Urry & Padovani 1995).

Traditionally BL Lacs have been discovered in either radio or X-ray band, which led to their classification as radio-selected (RBL) and X-ray-selected (XBL) BL Lacs. Best-known RBL samples include the 1Jy (Stickel et al. 1991), S4 (Stickel & Kühr 1994) and S5 (Kühr & Schmidt 1990) samples and among the most important XBL samples are the EMSS (Gioia et al. 1990; Stocke et al. 1991) and Slew Survey (Perlman et al. 1996).

The two classes have different properties: RBLs are more variable, more luminous at radio and optical wavelengths and have a higher polarization (Stocke et al. 1985; Jannuzi et al. 1994). XBLs have a higher starlight fraction, 30–50 % (Stocke et al. 1985), and their morphology is less core-dominated in the radio than that of RBLs (Perlman & Stocke 1993). Due to these differences they were initially regarded as separate classes of AGN. However, in recent years samples including intermediate objects have been found in surveys which combine X-ray and radio observations. These include the RGB (RASS–Green Bank) sample (Laurent-Muehleisen et al. 1999), the Deep X-Ray Radio Blazar Survey (DXRBS) (Perlman et al. 1998; Landt et al. 2001) and the REX Survey (Caccianiga et al. 1999). Their discovery has strengthened the view that the BL Lac population is continuous and RBLs and XBLs represent the opposite ends of the continuum. The reason for such a continuity lies in the cutoff frequency of the synchrotron component in the SED. The synchrotron peak frequency of RBLs is in the radio/IR band and for XBLs the peak is mostly in the UV/X-ray band (Giommi et al. 1995). The intermediate BL Lacs (IBL) have their synchrotron peak in the opti-

* e-mail: eni@kurp.hut.fi

cal wavelengths. This explains why they were not observed in the first surveys. Following the synchrotron cutoff model the terminology was brought to more physical ground: the RBL/XBL -division was replaced by division into low-energy-peaked BL Lacs (LBL) and high-energy-peaked BL Lacs (HBL) (Padovani & Giommi 1995). Most RBLs are LBLs and most XBLs are HBLs, but not all. The class boundaries can be loosely defined as $\nu_{peak} \approx 10^{13-14}$ Hz for LBLs, $\nu_{peak} \approx 10^{15-16}$ Hz for IBLs and $\nu_{peak} \approx 10^{17-18}$ Hz for HBLs.

Fossati et al. (1998) linked the shape of the SED and the synchrotron peak frequency to the source luminosity: the lower the peak frequency, the more luminous the source. This would mean that LBLs are intrinsically more luminous than HBLs. This sequencing is based on the absence of high-luminosity HBLs and low-luminosity LBLs. However, recently Giommi et al. (2005) reported the possible discovery of high-luminosity HBLs in the Sedentary Survey and evidence of low-power LBLs has also been discovered (Padovani et al. 2003; Caccianiga & Marchã 2004). These findings are at odds with the trend presented by Fossati et al.

Ghisellini (1999) suggested that there is a class of BL Lacs whose synchrotron peak lies at even higher frequencies than that of conventional HBLs, $\nu_{peak} > 10^{19}$ Hz. These objects can be called ultra-high-energy synchrotron peak BL Lacs (UHBLs) (Giommi et al. 2001). Following the dependency of the SED shape and luminosity, UHBLs are thought to be extremely faint at radio wavelengths which is why they have escaped notice. Extensive γ -ray observations are needed to unambiguously identify them.

In this paper we take a new approach to studying the properties of the BL Lac population. Our goal is to plot the SEDs of the Metsähovi Radio Observatory BL Lac sample, which comprises nearly 400 objects, including objects from all the best-known surveys at radio and X-ray wavelengths. This way we can examine the population properties of a sample with a wide range of attributes instead of focusing on one or two limited surveys.

The aim of this paper was to test both the continuity of the BL Lac population and the blazar sequence scenario, and to assign a SED-based classification to those objects that previously had none. A large database of flux measurements is collected and SEDs are plotted for more than 300 BL Lacs. Each object is classified as LBL, IBL or HBL. The relationship of synchrotron peak frequency and luminosities at several frequencies is also tested along with the properties of broad band spectral indices. Throughout this paper we assume $H_0 = 65 \text{ km s}^{-1} \text{ Mpc}^{-1}$ and $\Omega_0 = 1$. All statistical tests were carried out using Unistat 5.5 software.

2. The sample

The Metsähovi BL Lac sample includes 381 objects selected from the Veron-Cetty & Veron BL Lac Catalogue (Veron-Cetty & Veron 2000), hereafter VCV2000, and 17 objects from literature. Given the northern location of the Metsähovi observatory, the source with the lowest declination in the sample is PKS 2223-114 at $\delta = -11:13:41$. The list of

sample sources (table 3) is published electronically¹. A large part of the objects in VCV2000 are from well-known and well-defined samples such as the 1Jy, S4, S5, EMSS and Einstein Slew Survey. Also BL Lacs from the first release of DXRBS identifications (Perlman et al. 1998) are included. No selection criteria (other than declination) in addition to the ones in the original surveys were imposed on the sample. The aim was to examine the behaviour of an extensive sample containing all known BL Lacs up to the year 2000.

According to VCV2000 the Metsähovi BL Lac sample can be further classified as follows: 63 % are confirmed, 3 % probable and 8 % possible BL Lacs, 14 % are objects with high optical polarization and 12 % (including the BL Lacs taken from literature) lack any subclassification. In the sample there are 6 sources that are not in the later editions of Veron-Cetty & Veron BL Lac Catalogues (Veron-Cetty & Veron 2001, 2003). These objects have been excluded from the data analysis performed in this paper.

3. The data

In order to plot as accurate SEDs as possible, a large amount of data from several wavelengths was collected. Because simultaneous multifrequency flux measurements are not available, datapoints from different epochs were searched from databases and literature.

3.1. Radio data

The starting point in collecting radio data were the Metsähovi observations at 37 GHz from late 2001 to January 2004. The full data set and a more detailed analysis about the 37 GHz behaviour of the sample sources will be published in a forthcoming paper (Nieppola et al., in preparation for the A&A). Of the BL Lac sample 137 objects were detected at $\sigma \geq 4$. There were 255 BL Lacs that were not detected and 6 that had not been observed yet during the time mentioned. The limiting flux of the Metsähovi radio telescope is about 0.2 Jy under optimal weather conditions.

Our group has also obtained flux density data at higher radio frequencies from our observations with the Swedish-ESO Submillimetre Telescope (SEST) between 1987 and 2003 at 3 mm and 1.3 mm. For some objects we got data from the RATAN observatory at frequencies 2.3, 4.8, 7.7, 11.2, 21.8 and 30 GHz (Tornikoski et al., in preparation for the A&A). Additional low frequency datapoints were found in VCV2000 and WGA-catalogue (White et al. 1996).

The large majority of radio data were obtained from the Astrophysical Catalogues Support System (CATS) maintained by Special Astrophysical Observatory, Russia². The search results from CATS contained data from over 140 different catalogues and more than 100 radio frequencies.

¹ www.edpsciences.org

² <http://cats.sao.ru/>

3.2. Data from other frequency bands

The IR datapoints are from CATS, originating from IRAS- and 2MASS-catalogues. The wavelengths used are 1.25, 1.65, 2.0, 2.17, 12, 25, 60 and 100 μm .

The optical data also are mainly from CATS. Some datapoints from V-band were added from Donato et al. (2001).

The X-ray data are from Einstein- and ROSAT-catalogues. The majority is from WGACAT (White et al. 1996) and RBSC-catalogue (Voges et al. 1999). Datapoints were also collected from the following papers: Donato et al. (2001), Lamer et al. (1996) and Laurent-Muehleisen et al. (1999). EMSS-data were included as well (Gioia et al. 1990; Stocke et al. 1991).

All of the data from gamma region came from the Third EGRET Catalogue (Hartman et al. 1999). Such data were available for only 14 objects.

4. Computing the spectral energy distributions

For all sources with a sufficient number of datapoints a spectral energy distribution was plotted in the form $\log \nu - \log \nu F$. All frequencies used are observed frequencies, they have not been reduced to rest frame frequencies. The synchrotron component of the SED was fitted with a parabolic function

$$y = Ax^2 + Bx + C \quad (1)$$

in order to determine the synchrotron peak frequency $\nu_{peak} = -B/2A$. The fitting was successful for 304 objects; the rest were too sparsely sampled. The decision whether or not to include X-ray datapoints in the fit was based solely on a visual estimate for each individual object. All the SEDs (fig. 13) are published electronically. The synchrotron peak frequencies are shown in table 3 col. 5.

We note that using a simple parabolic function in the fitting produces some error especially among HBLs. In their case the X-ray datapoints are typically included in the rising synchrotron component, and therefore the parabola peaks after the X-ray domain. In reality, the synchrotron peak is expected to occur at or very close to the X-ray wavelengths and the decline to be more rapid. Thus the peak frequencies of the most extreme objects can be exaggerated.

The objects were assigned a LBL/IBL/HBL classification according to ν_{peak} . On the basis of the criteria of Padovani & Giommi (1995), we decided to draw the boundaries as follows: for LBLs, $\log \nu_{peak} < 14.5$, for IBLs $14.5 < \log \nu_{peak} < 16.5$ and for HBLs $\log \nu_{peak} > 16.5$. Thus the peak frequencies of LBLs stretch up to the optical region, IBLs peak in the optical and UV-bands and HBLs from soft X-rays upwards.

4.1. The distribution of ν_{peak}

When the objects were classified as LBL/IBL/HBL according to their ν_{peak} as described in the previous section, the division resulted in the three classes being almost equal in size. There were 98 LBLs, 96 IBLs and 110 HBLs. The distribution is smooth and decreases steadily towards the higher peak

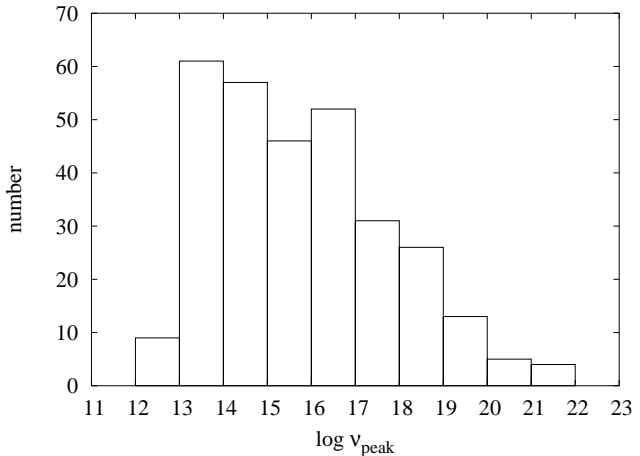


Fig. 1. The distribution of the synchrotron peak frequencies in the Metsähovi sample.

Table 1. Division of observational BL Lac classes to physical ones.

| | LBL | IBL | HBL |
|-----|------|------|------|
| RBL | 84 % | 10 % | 6 % |
| IBL | 22 % | 36 % | 42 % |
| XBL | 21 % | 25 % | 54 % |

frequencies (fig. 1). This can be a real effect, suggesting that sources in which electrons are accelerated to extreme energies are intrinsically rare, or due to selection effects in surveys. The frequency interval $\nu_{peak} = 10^{13-14}$ Hz is the most populated.

Table 1 presents how the classification with respect to the observational band relates to the one based on the SED. Here RBL classification has been assigned to objects in the 1Jy and S4 surveys, IBL to objects in RGB and 200 mJy BL Lac (Bondi et al. 2001) surveys and XBL to objects in the Einstein Slew Survey. This RBL/XBL classification has been adopted from Giommi et al. (1995). Among the 304 sources for which the SED could be plotted there were 31 RBLs, 115 IBLs and 48 XBLs. Several objects got multiple classifications.

Table 1 clearly demonstrates how surveys in the X-ray energies are more prone to find low-energy BL Lacs than radio surveys are to find HBLs. A large majority of RBLs really are LBLs. In fact, the 6 % of RBLs that turned out to be HBLs are the radio-luminous Mrk 421 and Mrk 501. Objects in the RGB and 200 mJy samples are more likely to be HBLs than LBLs, and only a third of them are truly intermediate. Of XBLs only half are HBLs and over 20 % are actually low-energy BL Lacs. These figures are certainly affected by the arbitrariness of the dividing boundaries between the classes, but the overall trend is expected to remain. It results from the fact that the X-ray luminosities of the samples in question are roughly the same whereas radio luminosities differ greatly.

4.2. UHBL candidates

As fig. 1 shows, there were several objects in the sample whose synchrotron peak frequency was extremely high. Usually ob-

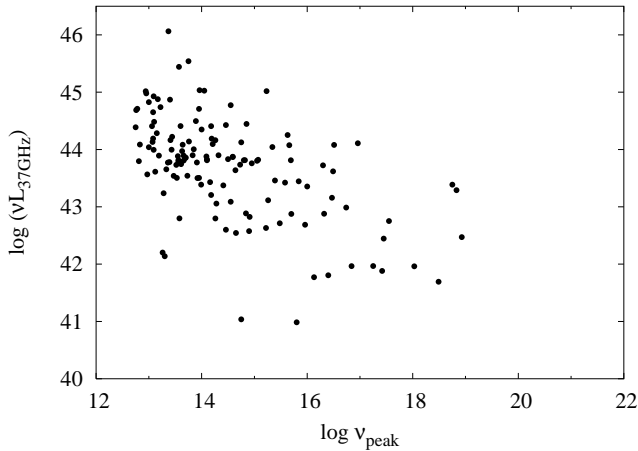


Fig. 2. Radio luminosity at 37 GHz plotted against synchrotron peak frequency.

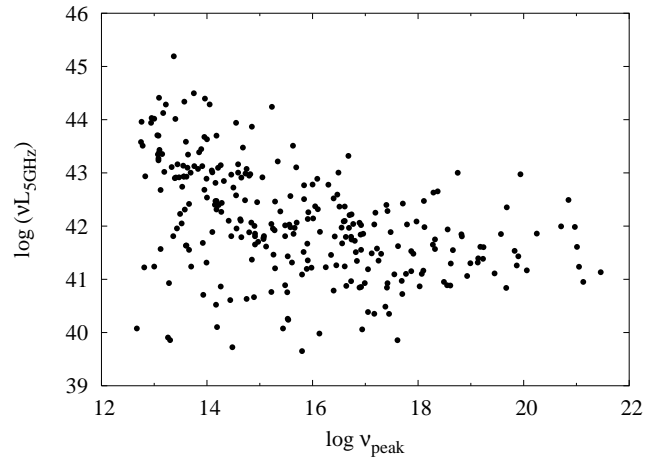


Fig. 3. Radio luminosity at 5 GHz plotted against synchrotron peak frequency.

jects with $\log \nu_{peak} > 17$ are considered as extreme, here the number of such objects was 80, approximately 26 % of all the fits. For 22 objects $\log \nu_{peak} > 19$ (table 2) and for 9 objects even $\log \nu_{peak} > 20$, corresponding to a peak energy of ~ 0.4 MeV. The SEDs of these sources are mainly very sparsely sampled, typically with datapoints from radio, optical and X-ray bands, and should be treated with caution. With that said, we note that even for objects with $\log \nu_{peak} > 20$ the datapoints fit very well on the rising parabolic function. We note again that the actual position of the peak is probably exaggerated by the use of a parabolic fitting function as mentioned in sect. 4. Therefore the peak frequencies of these objects cannot be considered as definite. Peaking near the MeV-region these sources would be excellent candidates for γ -observations.

5. Correlation between ν_{peak} and luminosity

5.1. High radio frequency (37 GHz)

Out of the three BL Lac classes, LBLs had 37 GHz detections for 81 % of the sources, IBLs for 36 % and HBLs for 12 %. This seems to indicate that most HBLs have a radio flux well below the flux limit of the Metsähovi telescope. This prompted us to study the possible correlation between the synchrotron peak frequency and 37 GHz source luminosity more closely.

To calculate the luminosities, redshift data was collected from VCV2000, Stocke et al. (1991), Laurent-Muehleisen et al. (1999), Donato et al. (2001) and SIMBAD database³. For sources which had no redshift available we used $z=0.4$. Both a detection at 37 GHz and synchrotron peak frequency ν_{peak} were available for 132 objects.

When the 37 GHz luminosity is plotted against the synchrotron peak frequency (fig. 2), the correlation is easily seen. LBLs are at the high-luminosity end of the plot and the luminosity drops towards the high-energy regime. According to Spearman Rank Correlation Test, there is significant negative correlation at the 99 % confidence level.

No real evidence of a population of low-luminosity LBLs or high-luminosity HBLs is found. However, there are two LBLs with almost as low luminosities as HBLs disrupting the declining trend. In addition, the lowest luminosities are not claimed by objects in the high end of the peak frequency range, but by two IBLs with $\log \nu_{peak} < 16$. The radio luminosities are widely scattered. An object with $\log \nu L = 44$ can have peak frequency values ranging from $\log \nu_{peak} = 13$ to $\log \nu_{peak} = 17$, approximately. Thus the radio luminosity cannot be used to determine the peak frequency of the source.

5.2. Low radio frequency (5 GHz)

The small number of HBL datapoints at 37 GHz convinced us to test the correlation also at 5 GHz. The number of available datapoints rose to 280. The correlation plot changed drastically (fig. 3). The most noticeable difference is the appearance of several low-luminosity LBLs (lower left of the figure). They even reach lower luminosities than any of the HBLs. The overall negative correlation is still present and significant at 99 % level. This differs from the result obtained by Padovani et al. (2003). However, their DXRBS BL Lac sample consisted of only 31 objects mainly representing the LBL/IBL end of the plot. This is the region with most scatter in our figure and within this limited area the correlation is less obvious even with a larger number of datapoints. Only when the whole range of values of $\log \nu_{peak}$ is considered the trend becomes evident.

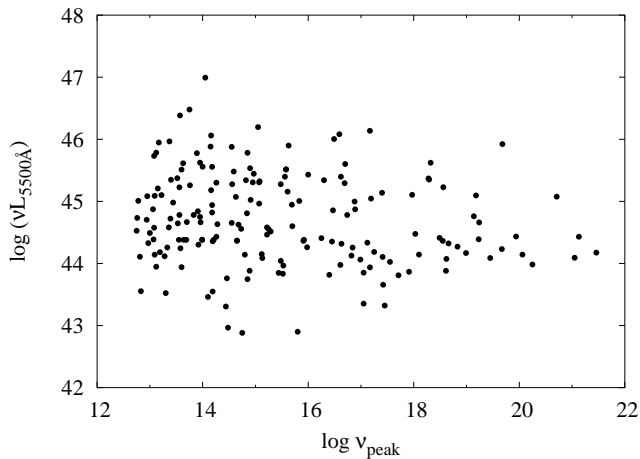
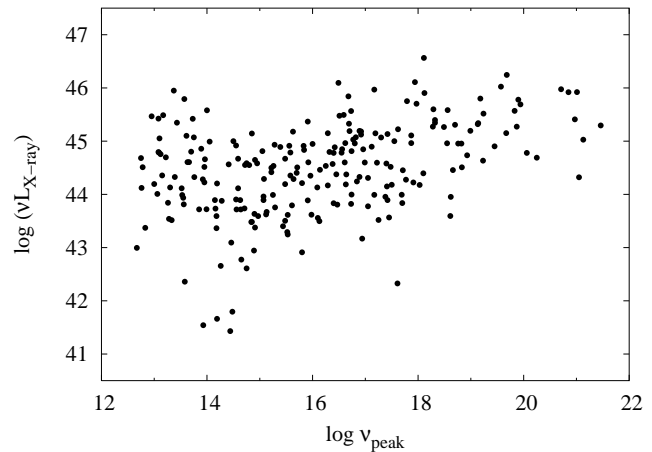
When compared with the corresponding figure of Fossati et al. (1998) our figure has much more scatter. A part of it is caused by a larger number of datapoints, but on closer examination our $\log \nu_{peak}$ values for the Slew Survey are much more widely spread. In Fossati et al. (1998) the Slew Survey objects have $\log \nu_{peak} = 15-19$, while in our study they have $\log \nu_{peak} \approx 13-21$. The 1Jy-sample takes on similar values of peak frequency in both studies.

We note that there is no evidence of very high-luminosity HBLs. In fact, the extreme HBLs adopt quite intermediate luminosity values avoiding also the low-luminosity region. However, the spectra of possible high-luminosity HBLs would

³ <http://simbad.u-strasbg.fr>.

Table 2. Objects for which $\log \nu_{peak} > 19$.

| Source | RA. (J2000) | Dec. (J2000) | $\log \nu_{peak}$ |
|------------------|-------------|--------------|-------------------|
| 1ES 0229+200 | 02:32:48.6 | +20:17:17 | 19.45 |
| RXS J0314.3+0620 | 03:14:23.9 | +06:19:57 | 19.57 |
| 2E 0323+0214 | 03:26:13.9 | +02:25:14 | 19.87 |
| 2E 0414+0057 | 04:16:52.4 | +01:05:24 | 20.71 |
| 1ES 0502+675 | 05:07:56.1 | +67:37:24 | 19.18 |
| EXO 0706.1+5913 | 07:10:30.1 | +59:08:21 | 21.05 |
| RXS J0847.2+1133 | 08:47:12.9 | +11:33:52 | 19.13 |
| 1ES 0927+500 | 09:30:37.5 | +49:50:25 | 21.13 |
| RXS J1008.1+4705 | 10:08:11.3 | +47:05:20 | 19.67 |
| RXS J1012.7+4229 | 10:12:44.3 | +42:29:57 | 20.97 |
| EXO 1449.9+2455 | 11:49:30.3 | +24:39:27 | 19.83 |
| PG 1218+304 | 12:21:21.9 | +30:10:37 | 19.14 |
| RXS J1319.5+1405 | 13:19:31.7 | +14:05:34 | 20.85 |
| RXS J1341.0+3959 | 13:41:05 | +39:59:45 | 20.06 |
| RXS J1353.4+5601 | 13:53:28 | +56:00:55 | 19.23 |
| RXS J1410.5+6100 | 14:10:31.7 | +61:00:10 | 20.25 |
| 2E 1415+2557 | 14:17:56.6 | +25:43:25 | 19.24 |
| RXS J1456.0+5048 | 14:56:03.7 | +50:48:25 | 19.94 |
| RXS J1458.4+4832 | 14:58:28 | +48:32:40 | 21.46 |
| 1ES 1533+535 | 15:35:00.8 | +53:20:37 | 19.68 |
| RXS J1756.2+5522 | 17:56:15.9 | +55:22:18 | 19.90 |
| RXS J2304.6+3705 | 23:04:36.6 | +37:05:08 | 21.01 |

**Fig. 4.** Optical luminosity at 5500 Å plotted against synchrotron peak frequency.**Fig. 5.** X-ray luminosity at 1 keV and ROSAT band plotted against synchrotron peak frequency.

very likely be totally featureless because of the powerful nucleus and thus the object would lack a redshift estimation. Therefore the redshift value assigned to featureless sources could have a big impact on the luminosity correlations and the appearance of high-luminosity HBLs (see section 5.6).

5.3. Optical region (5500 Å)

Figure 4 shows the optical luminosity at wavelength 5500 Å plotted against $\log \nu_{peak}$. There is a significant, slightly negative correlation present at 95 % level. We see again that LBLs have more scatter than HBLs. Overall, the correlation is much less evident than in the case of radio luminosity.

5.4. X-ray region

In fig. 5 we have plotted the correlation between X-ray luminosity and $\log \nu_{peak}$. In calculating the luminosities we have used both 1 keV data and data from the ROSAT band (0.1–2.4 keV). The error produced by the bandwidth difference is negligible when only the statistical properties of a large sample are considered. We note that in the case of X-ray luminosity, the correlation is positive and significant at 99 % level. This is in contrast with the blazar sequence scenario. Fossati et al. (1998) state that the overall luminosity of HBLs is lower than that of LBLs (see their fig. 12). While they admit that in the X-ray band objects exhibit complex behaviour, the systematic rising trend presented by our findings is not predicted.

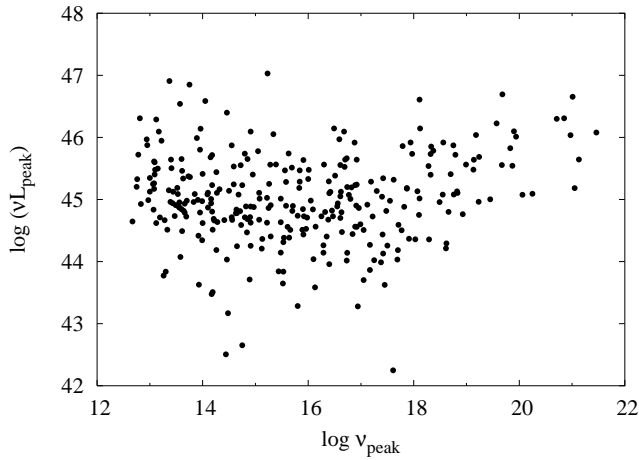


Fig. 6. Luminosity at the synchrotron peak frequency plotted against synchrotron peak frequency.

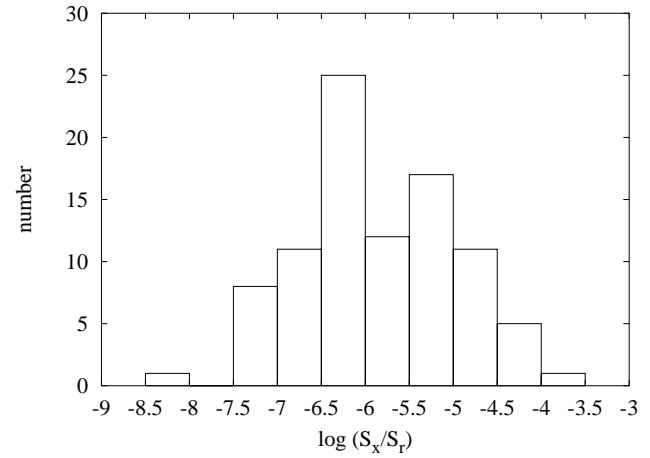


Fig. 7. The distribution of $\log (S_x/S_r)$.

5.5. Peak luminosity L_{peak}

In addition to luminosities at defined frequency bands, we calculated for each source its luminosity at the synchrotron peak frequency. This is plotted against $\log v_{peak}$ in fig. 6. There is no significant correlation. Therefore we can decisively say that the source luminosity does not depend on the synchrotron peak frequency. Fig. 7 of Fossati et al. (1998) also shows the dependence of L_{peak} and $\log v_{peak}$. In their study there is a significant, yet weak correlation. Again, we remark that a larger number of datapoints and a wider range of $\log v_{peak}$ reveal the true behaviour of the population and the lack of correlation. If only objects with $\log v_{peak} < 17$ are considered, there is a weak negative correlation also in our sample. On the other hand, when the high-energy tail with $\log v_{peak} > 17$ is tested, we find a significant positive correlation. Therefore the distribution almost seems to assume a concave shape.

5.6. The effect of z on luminosity correlations

Giommi et al. (2005) found numerous candidates for high-luminosity HBLs in the Sedentary Survey. All these objects seemed to reside at high redshifts ($z \geq 0.7$). In our luminosity calculations we assumed $z = 0.4$ for featureless objects, which is a low value compared to Giommi et al. Using a too low redshift value for a significant part of the sources would lead to a serious underestimation of luminosities. To take this into account, we tested the luminosity correlations also by assigning redshifts $z = 0.7$, $z = 1$ and $z = 1.5$ to those objects that had none.

The effect was most pronounced in the case of radio luminosities at 5 and 37 GHz. The number of relatively high-luminosity HBLs increased with the higher assumed redshift. However, only at very high redshift values ($z = 1$ or $z = 1.5$) the luminosities of a few HBLs became roughly comparable to those of LBLs. Considering the population average, $z_{av} = 0.33$, it is questionable whether all featureless sources would have $z \geq 1$, although for some of them this may be the case. Therefore, while the existence of high-luminosity HBLs

in this sample is possible, we do not expect the correlations to be affected by them.

In other frequency bands than radio, the effect of an increasing redshift was negligible. The shape of the correlations did not change notably, only the scatter increased somewhat. We note that in all wavelengths and for all assumed redshift values the significance of the statistical correlations remained the same.

6. Other properties of the sample

6.1. $\log (S_x/S_r)$ -distribution

The $\log (S_x/S_r)$ -distribution has traditionally been used to point out the bimodality in the BL Lac population. The dividing line between RBLs and XBLs has been $\log (S_x/S_r) = -5.5$ (Laurent-Muehleisen et al. 1999), when the fluxes are in the same units and X-ray and radio frequencies are 0.1–2.4 keV and 5 GHz respectively. Here we calculated the distribution to check the assumed continuity of the sample. X-ray fluxes are from the ROSAT band 0.1–2.4 keV and radio measurements are from Metsähovi at 37 GHz. If there was more than one flux measurement from one frequency, the average value was used.

The distribution is indeed unbroken with an average of $\log (S_x/S_r) = -5.85$ (fig. 7). The most populated interval is $\log (S_x/S_r) = [-6, -6.5]$. Pertaining to the unbalanced detection rates at 37 GHz, LBLs are overrepresented compared to HBLs in the plot. Only 14 % of the objects are HBLs. When considered separately, LBLs, IBLs and HBLs move progressively from low to higher values of $\log (S_x/S_r)$. There is substantial overlap between the distributions. The average values are -6.35 , -5.50 and -4.85 for LBLs, IBLs and HBLs respectively.

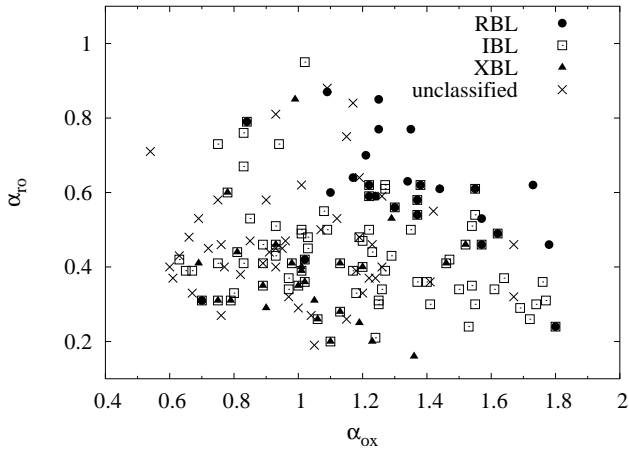


Fig. 8. The colour plane: α_{ro} plotted against α_{ox} . Frequency intervals 5 GHz–5500 Å–1 keV, ROSAT band. Different symbols denote the observational classification of BL Lacs.

6.2. Broad band spectral indices

6.2.1. The $\alpha_{ro} - \alpha_{ox}$ diagram

We calculated broad band spectral indices α_{ro} and α_{ox} to plot the sample in α_{ro} vs. α_{ox} diagram. Here the spectral index is defined as

$$\alpha_{1-2} = -\frac{\log(S_1/S_2)}{\log(\nu_1/\nu_2)} \quad (2)$$

where S_1 and S_2 are the fluxes in frequencies ν_1 and ν_2 respectively and $S_\nu = \nu^{-\alpha}$.

The α_{ro} vs. α_{ox} diagram has also been used as a means to demonstrate the division of the population. Generally, XBLs have lower values of both indices occupying the lower left corner of the plot, whereas RBLs lie in the upper right corner (Stocke et al. 1985; Laurent-Muehleisen et al. 1999). IBLs seem to have bridged the gap having intermediate values of both indices.

For comparison, we plotted two diagrams; one with low radio frequency (5 GHz) (fig. 8) and one with high radio frequency (37 GHz) (fig. 9). The optical wavelength used was 5500 Å. In both diagrams we used X-ray data at 1 keV from literature and, in addition, data from ROSAT band 0.1–2.4 keV. The error produced by the bandwidth difference is small compared with the benefits of a larger number of datapoints.

When the lower radio frequency is used (fig. 8), the indices for the whole population are $\alpha_{ox} = 0.54$ –1.8 and $\alpha_{ro} = 0.16$ –0.95. RBLs and XBLs occupy their expected locations but overall the distribution is even.

As for the higher radio frequency diagram (fig. 9), the intervals are slightly different; $\alpha_{ox} = 0.63$ –1.8 and $\alpha_{ro} = 0.29$ –1.13. The values of α_{ox} are the same as in fig. 8, but the number of datapoints is smaller. Here we note again the lack of HBLs compared to LBLs. This is why the lower left corner of fig. 9 is underpopulated compared with fig. 8.

We also plotted the diagram with 5 GHz showing the LBL/IBL/HBL classification of our study (fig. 10). It clearly shows how the transition of the synchrotron peak from LBL

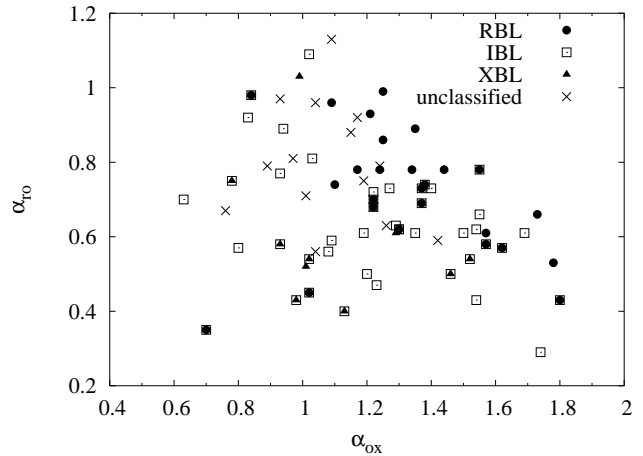


Fig. 9. The colour plane: α_{ro} plotted against α_{ox} . Frequency intervals 37 GHz–5500 Å–1 keV, ROSAT band. Different symbols denote the observational classification of BL Lacs.

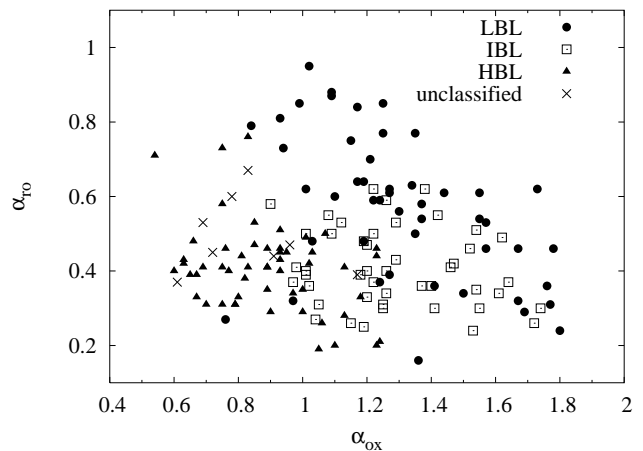


Fig. 10. The colour plane: α_{ro} plotted against α_{ox} . Frequency intervals 5 GHz–5500 Å–1 keV, ROSAT band. Different symbols denote the physical classification of BL Lacs obtained in this study.

to HBL moves the object on the $\alpha_{ro} - \alpha_{ox}$ -plane from the top to lower right and onwards to lower left, as described by Padovani & Giommi (1995). However, there are several LBLs that appear on the wrong side of the $\alpha_{rx} = 0.75$ line that has usually been thought of as a dividing line between LBLs and HBLs. This suggests that the $\alpha_{rx} = 0.75$ divide is not very effective and LBLs take on very scattered values of α_{ro} .

There are some objects in the $\alpha_{ro} - \alpha_{ox}$ -plot (fig. 10) with no classification (marked with x). They are concentrated in quite a small area with $\alpha_{ox} = 0.61$ –1.17 and $\alpha_{ro} = 0.37$ –0.67. Their synchrotron peak frequencies have not been calculated on account of very poor fits, but judging by their spectral indices they are likely to be HBLs.

6.2.2. α_{rx} vs. $\log \nu_{peak}$

The relation between α_{rx} and $\log \nu_{peak}$ is shown in fig. 11. We used radio frequency 5 GHz and X-ray data comes pri-

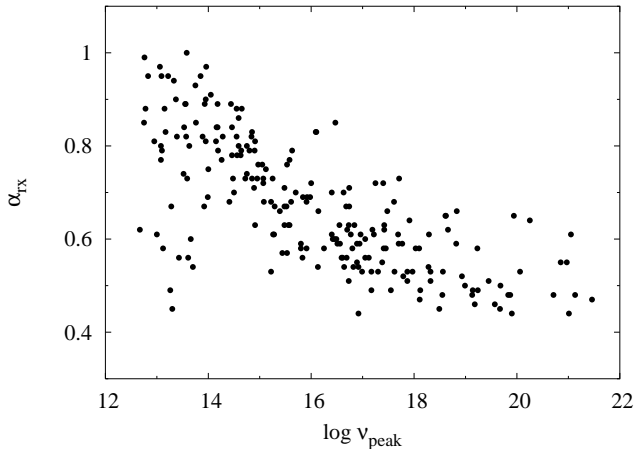


Fig. 11. Radio-X-ray spectral index α_{rx} plotted against synchrotron peak frequency.

marily from 1 keV. For those objects that have no 1 keV flux available we used data from the ROSAT band. According to the Spearman rank correlation test, the negative correlation is significant at 99 % level. However, the correlation seems to break apart at $\log \nu_{peak} < 14$. LBLs take on α_{rx} -values between 0.45–1. Fossati et al. (1998) suggested that the correlation between the radio luminosity and X-ray luminosity in the rising Compton–component makes α_{rx} tend to a fixed value when $\log \nu_{peak} < 14$, but in our plot this seems not to be the case.

When $\log \nu_{peak} > 14$ the correlation is apparent. This speaks for the authenticity of the UHBL candidates, as they take their place at the end of the continuum with low spectral index values. All objects with $\log \nu_{peak} > 19$ also have $\alpha_{rx} \leq 0.65$.

From the α_{rx} vs. $\log \nu_{peak}$ -plot we can see that assigning an object an LBL/HBL classification based only on the value of α_{rx} is risky. While object with $\alpha_{rx} > 0.75$ is very likely an LBL, the opposite does not hold. In fact, approximately 30 % of objects with $\alpha_{rx} < 0.75$ have $\log \nu_{peak} < 16$. At $\alpha_{rx} \approx 0.6$ the possible values of ν_{peak} span across as much as eight magnitudes.

When compared with the corresponding figures of Fossati et al. (1998) and Padovani et al. (2003), our plot seems to be a combination of the two. This is explained by the fact that both the samples used by Fossati et al. (1Jy and Slew Survey) and part of the sample used by Padovani et al. (DXRBS) are included in the Metsähovi sample. Thereby we see a strong correlation with a substantial increase in scatter of the α_{rx} -values towards the lower end. We stress that our data considerably extends the range of values of $\log \nu_{peak}$.

6.2.3. α_{ro} vs. $\log \nu_{peak}$

The correlation between the spectral index between radio (5 GHz) and optical (5500 Å) frequencies and synchrotron peak frequency is shown in fig. 12. The overall trend is easily seen, changing from the steep negative correlation of LBLs to an almost constant trend of HBLs. The change occurs roughly when the synchrotron peak of the SED moves to frequencies higher

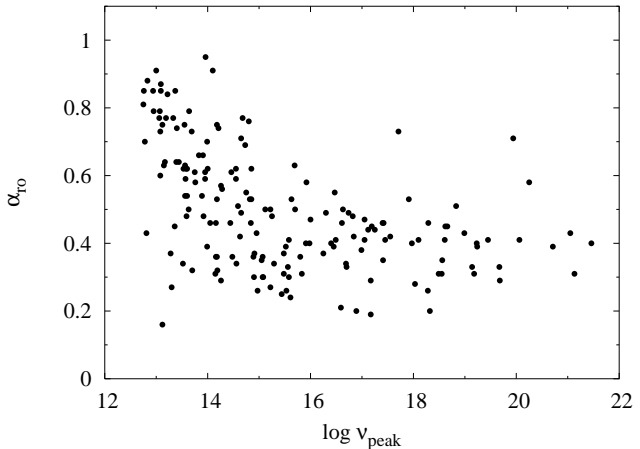


Fig. 12. Radio-optical spectral index α_{ro} plotted against synchrotron peak frequency.

than those used to calculate α_{ro} . After that point, the peak frequency no longer has an influence on α_{ro} . The negative correlation is significant at 99 % level. Again, however, we see a few points breaking this scenario, both LBLs with very low values of α_{ro} and HBLs with high values of α_{ro} .

We note that, as in the case of α_{rx} , the scatter in the figure is significant. Therefore the value of α_{ro} cannot be reliably used to classify BL Lacs. Only if α_{ro} is very close to one, the object is likely to be an LBL.

7. Discussion

Our findings support the results of Costamante et al. (2001). Their study concludes that objects 1ES 0033+595, 1ES 0120+340, 1ES 1218+304 and 1ES 1426+428 are extreme HBLs with synchrotron peak frequencies exceeding 10^{18} Hz. Our results show that they all peak at roughly $\log \nu_{peak} \approx 19$. Meanwhile, the extreme nature of 1ES 2344+514 (Giommi et al. 2000) is not revealed in our study as it had a peak frequency of $\log \nu_{peak} = 16.4$. Giommi et al. state that it is indeed very variable, with synchrotron peak frequencies ranging from $\log \nu_{peak} \approx 17$ to $\log \nu_{peak} \approx 18$. Mrk 501 is another example of a variable source; its synchrotron peak has been as high as $\log \nu_{peak} \approx 19$ (Pian et al. 1998), but the peak in our SED occurred at $\log \nu_{peak} \approx 16.84$.

In this paper we tested the correlation between the synchrotron peak frequency and luminosities at radio, optical and X-ray wavelengths and luminosity at the synchrotron peak of each source. According to the blazar sequence scenario promoted by Fossati et al. (1998), HBLs have lower luminosities at all wavelengths. In the X-ray region, in the SED of LBLs the synchrotron and SSC-components meet resulting in a concave X-ray spectrum. In HBLs the synchrotron component peaks at or near the X-ray energies. Because the SEDs of LBLs and HBLs are so differently shaped in this frequency band, the X-ray correlation may be less significant. Still, on the whole, LBLs are expected to be more luminous. When the defined frequency bands are considered, our data seems to support this scenario in all other frequencies except in X-rays. There we

find a clear positive correlation which contradicts the blazar sequence. Luminosities rise towards the high peak frequencies. When all luminosity vs. $\log \nu_{peak}$ correlations are studied simultaneously, a kind of sequence is revealed: at radio frequencies the negative correlation is steep, in optical wavelengths the correlation is only slightly negative and in the X-ray region it turns positive. However, the negative correlation of luminosity at 5 GHz and synchrotron peak frequency is expected to originate solely from the shifting of the bulk of the synchrotron emission to the higher frequencies with growing $\log \nu_{peak}$ and as such does not authenticate the interdependence of source luminosity and peak frequency. A negative luminosity correlation at 5 GHz and a positive one at X-rays is what we would expect if the only changing parameter in the SED sequence was ν_{peak} . When source luminosities at synchrotron peak frequencies are calculated, we find that they do not correlate with $\log \nu_{peak}$.

In addition to the positive correlation of X-ray luminosity and synchrotron peak and the lack of synchrotron luminosity correlation, the blazar sequence scenario is brought into question by the appearance of numerous low-luminosity LBLs at 5 GHz. The faintest LBLs reach even lower luminosities than most of the HBLs. As the 5 GHz flux limit of even the least limited radio-selected sample, RGB, is 20 mJy, it is obvious that these objects have been identified for the most part from X-ray surveys. We note that there are some 5 GHz low-luminosity LBLs that have a detection at 37 GHz. Especially for these sources we have to consider the possibility that the 5 GHz flux measurement is from a particularly quiescent state and does not represent the object accurately. Padovani et al. (2003) found low-luminosity LBLs among the DXRBS BL Lacs. In our low-luminosity LBLs there are 4 objects from the DXRBS survey.

The 5 GHz low-luminosity LBLs appear also in luminosity plots from other frequency bands, again, in the low-luminosity end. All the extreme HBLs have relatively high or intermediate luminosities. This effect, especially in X-rays, seems to support the scenario that UHBLs are in fact a rare class. If they were common and X-ray luminous, the numerous X-ray surveys performed lately should have detected them in large numbers. On the whole, the scatter in luminosities diminishes towards higher peak frequencies at all wavelengths. There is no solid evidence of truly high-luminosity HBLs with a measured redshift in radio wavelengths. The high-luminosity HBLs reported by Giommi et al. (2005) are from the Sedentary Survey which is not included in our sample.

We find that the low-luminosity LBLs behave abnormally also on the broad band spectral index plots, α_{ro} vs. α_{ox} , α_{rx} vs. $\log \nu_{peak}$ and α_{ro} vs. $\log \nu_{peak}$. In the first the BL Lac classes take their expected places except for a few of the low-luminosity LBLs that invade the region usually populated by HBLs. Doing so, they cross the $\alpha_{rx} = 0.75$ border frequently used to classify BL Lacs to LBLs and HBLs.

When the α_{rx} vs. $\log \nu_{peak}$ -plot is examined, we find a strong negative correlation, but LBLs ($\log \nu_{peak} < 14$) disrupt the trend and take on values $\alpha_{rx} = 0.45-1$. Hints of such a distribution was discovered by Padovani et al. (2003), but the wider range of $\log \nu_{peak}$ in our sample makes it evident. All LBLs with conspicuously low α_{rx} are among the low-luminosity LBLs in the 5 GHz luminosity plot. We considered the possibility that

the low indices in these objects are due to the wider bandwidth of the ROSAT fluxes compared to the 1 keV fluxes, but this seems to have little effect. For those objects that had α_{rx} computed for both X-ray energies, we calculated the average values of both indices. The average for ROSAT band α_{rx} was 0.63 while for 1 keV fluxes it was 0.69. This difference is small compared to the deviation of the low- α_{rx} LBLs from their expected location. Also for 3 of the 10 LBLs with lowest α_{rx} -values 1 keV flux has been used in calculating the spectral index.

In α_{ro} vs. $\log \nu_{peak}$ -plot LBLs behave in a similar way, at $\log \nu_{peak} \approx 13$ they have $\alpha_{ro} = 0.16-0.95$. In this plot we also see 3 HBLs with conspicuously high α_{ro} . They have relatively high radio luminosities and low optical luminosities. Each source has only one flux measurement at 5500 Å, possibly from an anomalously quiescent state. For these HBLs we also considered the possibility that their X-ray flux actually originates from IC rather than synchrotron radiation. This would lower their peak frequencies and move them left on the α_{ro} vs. $\log \nu_{peak}$ -plane. For two of them (RXS J1456.0+5048, $\log \nu_{peak} = 19.94$ and RXS J1410.5+6100, $\log \nu_{peak} = 20.25$) this seems possible albeit uncertain.

As explained before, when there are few datapoints representing the SED, the peak frequency is easily overestimated in the case of extreme HBLs. This affects also the luminosity correlations. However we do not expect the significance of the correlations at defined wavelengths to change, even if the datapoints in the high-energy end moved to the left. The only case where the consequences could be substantial is the $\log L_{peak}$ vs. $\log \nu_{peak}$ -plot (fig. 6). If the peak frequency is exaggerated, so is the luminosity at peak frequency. Thus the uncertain datapoints can move from upper right to lower left, possibly changing the correlation. We tested this by artificially lowering the peak luminosities of those sources whose νF_{peak} was notably higher in the SED than their X-ray flux, νF_{X-ray} . We changed their peak frequencies accordingly, and the highest $\log \nu_{peak}$ in the sample changed from 21.46 to 19.44. Yet the overall shape of the plot did not change enough to produce significant correlation. Therefore we find it unlikely that the overestimation of the $\log \nu_{peak}$ of HBLs affects the main results of this study.

8. Conclusions

In this paper we collected a large amount of multifrequency data as well as new flux measurements at 37 GHz and plotted the spectral energy distributions of over 300 BL Lacs of the Metsähovi BL Lac sample. Using such an extensive sample allowed us to detect the whole range of synchrotron peak frequencies reaching up to the MeV-region. The main conclusions are as follows:

1. For 22 objects we find that $\log \nu_{peak} > 19$. This high-frequency tail of the ν_{peak} distribution is unrepresented in most previous studies, but we find it essential for determining the properties of the population accurately.
2. The positive correlation of X-ray luminosity and synchrotron peak frequency and the lack of correlation between the source luminosity at synchrotron peak and peak frequency contradict the blazar sequence scenario. The differences between LBLs and HBLs cannot be attributed to unequal luminosities.

3. When the broad band spectral indices α_{rx} and α_{ro} are plotted against $\log \nu_{peak}$ we find substantial scatter in the figures. This implies that the values of α_{rx} and α_{ro} cannot be reliably used in BL Lac classification.

4. Based on the smooth, declining distribution of ν_{peak} and the lack of any bimodality in all other tests and calculations, we conclude that the BL Lac population as a whole is continuous and undivided.

Acknowledgements. We gratefully acknowledge the funding received from the Academy of Finland for our Metsähovi and SEST observing projects (project numbers 205969, 46341 and 51436). E.N. thanks Ilona Torniaainen for help in producing the SED plots for publication.

References

- Bondi, M., Marchã, M. J. M., Dallacasa, D., & Stanghellini, C. 2001, MNRAS, 325, 1109
- Caccianiga, A., Maccacaro, T., Wolter, A., della Ceca, R., & Gioia, I. M. 1999, ApJ, 513, 51
- Caccianiga, A. & Marchã, M. J. M. 2004, MNRAS, 348, 937
- Costamante, L., Ghisellini, G., Giommi, P., et al. 2001, A&A, 371, 512
- Donato, D., Ghisellini, G., Tagliaferri, G., & Fossati, G. 2001, A&A, 375, 739
- Fossati, G., Maraschi, L., Celotti, A., Comastri, A., & Ghisellini, G. 1998, MNRAS, 299, 433
- Ghisellini, G. 1999, ApL&C, 39, 17
- Gioia, I., Maccacaro, T., Schild, R., et al. 1990, ApJS, 72, 567
- Giommi, P., Ansari, S. G., & Micol, A. 1995, A&AS, 109, 267
- Giommi, P., Ghisellini, G., Padovani, P., & Tagliaferri, G. 2001, AIPC, 599, 441
- Giommi, P., Padovani, P., & Perlman, E. 2000, MNRAS, 317, 743
- Giommi, P., Piranomonte, S., Perri, M., & Padovani, P. 2005, A&A, 434, 385
- Hartman, R. C., Bertsch, D. L., Bloom, S. D., et al. 1999, ApJS, 123, 79
- Jannuzi, B. T., Smith, P. S., & Elston, R. 1994, ApJ, 428, 130
- Kühr, H. & Schmidt, G. 1990, AJ, 99, 1
- Lamer, G., Brunner, H., & Staubert, R. 1996, A&A, 311, 384
- Landt, H., Padovani, P., Perlman, E. S., et al. 2001, MNRAS, 323, 757
- Laurent-Muehleisen, S. A., Kollgaard, R. I., Feigelson, E. D., Brinkmann, W., & Siebert, J. 1999, ApJ, 525, 127
- Padovani, P. & Giommi, P. 1995, ApJ, 444, 567
- Padovani, P., Perlman, E. S., Landt, H., Giommi, P., & Perri, M. 2003, ApJ, 588, 128
- Perlman, E. S., Padovani, P., Giommi, P., et al. 1998, AJ, 115, 1253
- Perlman, E. S. & Stocke, J. T. 1993, ApJ, 406, 430
- Perlman, E. S., Stocke, J. T., Schachter, J. F., et al. 1996, ApJS, 104, 251
- Pian, E., Vacanti, G., Tagliaferri, G., et al. 1998, ApJ, 492, 17
- Stickel, M. & Kühr, H. 1994, A&AS, 103, 349
- Stickel, M., Padovani, P., Urry, C. M., Fried, J. W., & Kühr, H. 1991, ApJ, 374, 431
- Stocke, J. T., Liebert, J., Schmidt, G., et al. 1985, ApJ, 298, 619
- Stocke, J. T., Morris, S. L., Gioia, I. M., et al. 1991, ApJS, 76, 813
- Urry, C. M. & Padovani, P. 1995, PASP, 107, 715
- Veron-Cetty, M. P. & Veron, P. 2000, ESOSR, 19, 1
- Veron-Cetty, M. P. & Veron, P. 2001, A&A, 374, 92
- Veron-Cetty, M. P. & Veron, P. 2003, A&A, 412, 399
- Voges, W., Aschenbach, B., Boller, T., et al. 1999, A&A, 349, 389
- White, N. E., Giommi, P., & Angelini, L. 1996, VizieR Online Data Catalogue IX/12, 9012, 0

Online Material

Table 3. The Metsähovi BL Lac sample. The synchrotron peak frequency and subsequent classification designated in this study are included when available.

| Source | RA.(J2000) | Dec.(J2000) | $\log \nu_{peak}$ | Class |
|------------------|------------|-------------|-------------------|-------|
| NRAO 5 | 00:06:13.9 | -06:23:36 | 12.75 | LBL |
| RX J0007.9+4711 | 00:07:59.9 | 47:12:07 | 16.14 | IBL |
| MS 0011.7+0837 | 00:14:19.7 | 08:54:04 | 16.74 | HBL |
| RXS J0018.4+2947 | 00:18:27.8 | 29:47:32 | - | - |
| PKS 0017+200 | 00:19:37.9 | 20:21:46 | 13.08 | LBL |
| PKS 0019+058 | 00:22:32.5 | 06:08:05 | 13.19 | LBL |
| RXS J0325.2+1515 | 00:35:14.9 | 15:15:04 | 13.73 | LBL |
| 1ES 0033+595 | 00:35:52.6 | 59:50:04 | 18.93 | HBL |
| 1ES 0037+405 | 00:40:13.8 | 40:50:04 | 16.8 | HBL |
| RXS J0045.3+2127 | 00:45:19.1 | 21:27:43 | 16.89 | HBL |
| B3 0045+395 | 00:47:55.2 | 39:48:57 | - | - |
| EXO 0044.4+2001 | 00:47:08 | 20:17:44 | 16.05 | IBL |
| PKS 0047+023 | 00:49:43.3 | 02:37:04 | 13.56 | LBL |
| PKS 0048-097 | 00:50:41.2 | -09:29:06 | 13.39 | LBL |
| NPM1G -09.0033 | 00:56:20 | -09:36:32 | - | - |
| RXS J0058.2+1723 | 00:58:16.8 | 17:23:14 | - | - |
| Q J0109+181 | 01:09:08.1 | 18:16:03 | - | - |
| NPM1G +41.0022 | 01:10:04.8 | 41:49:50 | 17.7 | HBL |
| RXS J0111.5+0536 | 01:11:30.1 | 05:36:28 | - | - |
| S2 0109+22 | 01:12:05.8 | 22:44:39 | 13.59 | LBL |
| RXS J0115.7+2519 | 01:15:46.5 | 25:19:57 | 13.43 | LBL |
| 1ES 0120+340 | 01:23:08.7 | 34:20:51 | 18.32 | HBL |
| MS 0122.1+0903 | 01:24:44.5 | 09:18:49 | 15.53 | IBL |
| B3 0133+388 | 01:36:32.6 | 39:06:00 | 16.59 | HBL |
| PKS 0139-09 | 01:41:25.8 | -09:28:43 | 13.4 | LBL |
| 1ES 0145+138 | 01:48:29.7 | 14:02:18 | 15.44 | IBL |
| NPM1G +01.0067 | 01:52:39.6 | 01:47:17 | - | - |
| 8C 0149+710 | 01:53:25.8 | 71:15:07 | 14.75 | IBL |
| RXS J0155.9+1502 | 01:56:00.3 | 15:02:13 | - | - |
| 87GB 01569+1032 | 01:59:34.4 | 10:47:07 | 15.56 | IBL |
| RXS J0200.4+2712 | 02:00:29.5 | 27:12:36 | - | - |
| MS 0158.5+0019 | 02:01:06.1 | 00:34:00 | 17.87 | HBL |
| RXS J0202.4+0849 | 02:02:26.4 | 08:49:12 | - | - |
| S5 0159+72 | 02:03:33.3 | 72:32:53 | 13.99 | LBL |
| MS 0205.7+3509 | 02:08:38.2 | 35:23:13 | 15.22 | IBL |
| 87GB 02109+5130 | 02:14:17.9 | 51:44:52 | 17.69 | HBL |
| RXS J0216.5+2314 | 02:16:32.1 | 23:14:47 | - | - |
| Z 0214+083 | 02:17:17 | 08:37:03 | 15.23 | IBL |
| S4 0218+35 | 02:21:05.4 | 35:56:15 | - | - |
| 3C 66A | 02:22:39.6 | 43:02:08 | 15.63 | IBL |
| RXS J0227.2+0201 | 02:27:16.6 | 02:01:58 | - | - |
| 1ES 0229+200 | 02:32:48.6 | 20:17:17 | 19.45 | HBL |
| Q 0230+3429 | 02:33:20.3 | 34:42:54 | 15.84 | IBL |
| AO 0235+164 | 02:38:38.8 | 16:36:59 | 13.57 | LBL |
| S5 0238+71 | 02:43:31 | 71:20:18 | 16.3 | IBL |
| NPM1G +10.0097 | 02:45:13.5 | 10:47:23 | - | - |
| RXS J0250.6+1712 | 02:50:38 | 17:12:08 | - | - |
| MS 0257.9+3429 | 03:01:03.8 | 34:41:01 | 13.28 | LBL |
| 4C 47.08 | 03:03:35.2 | 47:16:17 | 14.18 | LBL |
| RXS J0303.5+0554 | 03:03:30.1 | 05:54:17 | - | - |
| PKS 0306+102 | 03:09:03.6 | 10:29:16 | 12.94 | LBL |
| VZw331 | 03:13:57.9 | 41:15:24 | 14.48 | LBL |
| RXS J0314.0+2445 | 03:14:02.7 | 24:44:31 | 12.67 | LBL |

Table 3. continued.

| Source | RA.(J2000) | Dec.(J2000) | $\log v_{peak}$ | Class |
|--------------------|------------|-------------|-----------------|-------|
| RXS J0314.3+0620 | 03:14:23.9 | 06:19:57 | 19.57 | HBL |
| RXS J0316.1+0904 | 03:16:12.9 | 09:04:43 | 15.91 | IBL |
| MS 03170+1834 | 03:19:51.8 | 18:45:35 | 16.99 | HBL |
| RGB J0321+2336 | 03:22:00 | 23:36:11 | - | - |
| 2E 0323+0214 | 03:26:13.9 | 02:25:14 | 19.87 | HBL |
| RXS J0331.3+0654 | 03:31:19.4 | 06:54:28 | - | - |
| RXS J0349.9+0640 | 03:49:59.7 | 06:40:56 | - | - |
| PKS 0406+121 | 04:09:22.1 | 12:17:39 | 13.22 | LBL |
| 2E 0414+0057 | 04:16:52.4 | 01:05:24 | 20.71 | HBL |
| 1WGA J0421.5+1433 | 04:21:33.1 | 14:33:54 | 13.93 | LBL |
| MS 0419.3+1943 | 04:22:18.5 | 19:50:53 | 16.82 | HBL |
| PKS 0420+022 | 04:22:52.2 | 02:19:27 | - | - |
| PKS 0422+004 | 04:24:46.8 | 00:36:07 | 15.69 | IBL |
| MCG 38364 | 04:25:51.3 | -08:33:38 | 17.17 | HBL |
| 2EG J0432+2910 | 04:33:37.7 | 29:05:56 | 14.09 | LBL |
| 1ES 0446+449 | 04:50:07.3 | 45:03:12 | - | - |
| PKS 0459+135 | 05:02:33.2 | 13:38:11 | 13.55 | LBL |
| Q 0458+6530 | 05:03:03.4 | 65:34:10 | 18.12 | HBL |
| RXS J0505.5+0416 | 05:05:34.7 | 04:15:54 | 16.94 | HBL |
| 1ES 0502+675 | 05:07:56.1 | 67:37:24 | 19.18 | HBL |
| S5 0454+84 | 05:08:42.5 | 84:32:05 | 13.58 | LBL |
| MG 0509+0541 | 05:09:25.9 | 05:41:35 | 15.34 | IBL |
| 4U 0506-03 | 05:09:39 | -04:00:36 | 17.94 | HBL |
| 2E 0514+0626 | 05:17:04 | 06:29:39 | - | - |
| 1ES 0525+713 | 05:31:41.7 | 71:22:17 | - | - |
| TEX 0554+534 | 05:58:11.6 | 53:28:19 | 14.44 | LBL |
| MS 0607.9+7108 | 06:13:42.8 | 71:07:29 | 14.85 | IBL |
| 87GB 06216+4441 | 06:25:18.3 | 44:40:02 | 13.61 | LBL |
| 1ES 0647+250 | 06:50:46.5 | 25:03:00 | 18.28 | HBL |
| B3 0651+428 | 06:54:43.5 | 42:47:59 | 15.12 | IBL |
| NPM1G +42.0131 | 06:56:10.6 | 42:37:02 | 17.25 | HBL |
| EXO 0706.1+5913 | 07:10:30.1 | 59:08:21 | 21.05 | HBL |
| RXS J0712.3+5719 | 07:12:18.7 | 57:19:22 | - | - |
| S5 0716+714 | 07:21:53.3 | 71:20:36 | 14.46 | LBL |
| RXS J0723.2+5841 | 07:23:13.2 | 58:41:23 | - | - |
| FIRST J0724.7+2621 | 07:24:42.8 | 26:21:30 | 16.39 | IBL |
| PKS 0723-008 | 07:25:50.7 | -00:54:56 | - | - |
| FIRST J0730.4+3307 | 07:30:26.1 | 33:07:22 | 16.29 | IBL |
| RXS J0737.3+3517 | 07:37:21 | 35:17:41 | 17.77 | HBL |
| FIRST J0738.6+3139 | 07:38:37.8 | 31:39:30 | - | - |
| PKS 0735+17 | 07:38:07.4 | 17:42:19 | 13.95 | LBL |
| FIRST J0741.3+2253 | 07:41:18.8 | 22:53:39 | - | - |
| MS 0737.9+7441 | 07:44:05.1 | 74:33:59 | 13.61 | LBL |
| S4 0749+54 | 07:53:01.3 | 53:53:00 | 13.12 | LBL |
| GB 0751+485 | 07:54:45.7 | 48:23:51 | 14.32 | LBL |
| PKS 0754+100 | 07:57:06.7 | 09:56:35 | 13.63 | LBL |
| RXS J0800.1+6210 | 08:00:06.5 | 62:10:12 | - | - |
| RXS J0801.0+6444 | 08:01:00.7 | 64:44:43 | - | - |
| RXS J0805.4+7534 | 08:05:26.5 | 75:34:25 | 15.96 | IBL |
| SBS 0802+596 | 08:06:25.9 | 59:31:07 | 16.69 | HBL |
| B2 0806+31 | 08:09:13.4 | 31:22:22 | - | - |
| RXS J0809.6+3455 | 08:09:38.5 | 34:55:37 | 18.29 | HBL |
| 1ES 0806+524 | 08:09:49.2 | 52:18:58 | 16.56 | HBL |
| PKS 0808+019 | 08:11:26.6 | 01:46:52 | 13.17 | LBL |

Table 3. continued.

| Source | RA.(J2000) | Dec.(J2000) | $\log \nu_{peak}$ | Class |
|--------------------|-------------|-------------|-------------------|-------|
| RXS J0812.1+5717 | 08:12:08.8 | 57:17:34 | - | - |
| EXO 0811.2+2949 | 08:14:21.8 | 29:40:32 | - | - |
| 1WGA J0816.0-0736 | 08:16:04.3 | -07:35:57 | 14.19 | LBL |
| RXS J0816.3+5739 | 08:16:23.8 | 57:39:03 | 17.19 | HBL |
| RXS J0816.6+6208 | 08:16:40.9 | 62:08:44 | 15.25 | IBL |
| OJ 425 | 08:18:16.1 | 42:22:46 | 13.33 | LBL |
| FIRST J0818.4+2814 | 08:18:27.3 | 28:14:02 | 16.01 | IBL |
| FIRST J0819.4+4037 | 08:19:25.8 | 40:37:43 | 16.61 | HBL |
| FIRST J0820.3+3640 | 08:20:20.2 | 36:40:04 | 14 | LBL |
| 4C 22.21 | 08:23:24.8 | 22:23:03 | 13.09 | LBL |
| PKS 0823+033 | 08:25:50.3 | 03:09:24 | 13.08 | LBL |
| RXS J0828.2+4153 | 08:28:14.2 | 41:53:50 | 18.66 | HBL |
| B3 0827+395 | 08:30:19.4 | 39:23:47 | - | - |
| PKS 0829+046 | 08:31:48.9 | 04:29:39 | 13.53 | LBL |
| 1H 0827+089 | 08:31:54.8 | 08:47:58 | 14.22 | LBL |
| OJ 448 | 08:32:23.2 | 49:13:21 | 13.06 | LBL |
| TEX 0836+182 | 08:39:30.7 | 18:02:47 | 14.55 | IBL |
| FIRST J0847.0+4117 | 08:47:02.5 | 41:17:57 | 18.11 | HBL |
| RXS J0847.2+1133 | 08:47:12.9 | 11:33:52 | 19.13 | HBL |
| RXS J0848.4+8111 | 08:48:27.8 | 81:11:47 | - | - |
| US 1889 | 08:54:09.9 | 44:08:31 | 17.42 | HBL |
| OJ 287 | 08:54:48.8 | 20:06:30 | 13.89 | LBL |
| NPM1G -09.0307 | 09:08:02.2 | -09:59:37 | 15.52 | IBL |
| B2 0906+31 | 09:09:53.3 | 31:06:03 | 17.4 | HBL |
| Ton 1015 | 09:10:37.1 | 33:29:24 | 15.39 | IBL |
| FIRST J0910.8+3902 | 09:10:52 | 39:02:02 | 18.33 | HBL |
| B2 0912+29 | 09:15:52.4 | 29:33:24 | 16 | IBL |
| RXS J0916.8+5238 | 09:16:52 | 52:38:28 | 17.22 | HBL |
| MS 0922.9+7459 | 09:28:02.6 | 74:47:19 | - | - |
| RXS J0929.2+5013 | 09:29:15.4 | 50:13:35 | 14.59 | IBL |
| S5 0916+86 | 09:29:42.7 | 86:12:21 | 14.16 | LBL |
| 1ES 0927+500 | 09:30:37.5 | 49:50:25 | 21.13 | HBL |
| B2 0927+35 | 09:30:55.3 | 35:03:38 | 14.8 | IBL |
| RXS J0930.9+3933 | 09:30:56.8 | 39:33:33 | - | - |
| SBS 0936+522 | 09:39:37.9 | 52:01:46 | - | - |
| B2 0937+26 | 09:40:13.6 | 26:03:26 | 14.75 | IBL |
| US 1015 | 09:50:11.8 | 45:53:20 | 15.48 | IBL |
| RGB J0952+656 | 09:52:32.2 | 65:38:01 | 15.08 | IBL |
| MS 0950.9+4929 | 09:54:09.8 | 49:15:00 | 16.92 | HBL |
| S4 0954+65 | 09:58:47.2 | 65:33:54 | 13.76 | LBL |
| 4C 22.25 | 10:00:21.36 | 22:33:07.4 | - | - |
| MS 0958.9+2102 | 10:01:42.4 | 20:48:18 | 15.54 | IBL |
| EXO 1004.0+3509 | 10:06:56.3 | 34:54:45 | 16.92 | HBL |
| RXS J10081+4705 | 10:08:11.3 | 47:05:20 | 19.67 | HBL |
| NRAO 350 | 10:12:13.3 | 06:30:57 | 16.09 | IBL |
| RXS J1012.7+4229 | 10:12:44.3 | 42:29:57 | 20.97 | HBL |
| GB 1011+496 | 10:15:04.2 | 49:26:01 | 16.74 | HBL |
| RXS J1016.2+4108 | 10:16:16.7 | 41:08:13 | 16.62 | HBL |
| RXS J1022.7-0112 | 10:22:43.9 | -01:12:56 | 17.97 | HBL |
| 1ES 1028+511 | 10:31:18.5 | 50:53:36 | 18.56 | HBL |
| FIRST J1032.6+3738 | 10:32:40.7 | 37:38:26 | - | - |
| RXS J1037.7+5711 | 10:37:44.2 | 57:11:57 | 14.95 | IBL |
| TEX 1040+244 | 10:43:09 | 24:08:35 | 13.1 | LBL |
| 1ES 1044+549 | 10:47:45.8 | 54:37:41 | 13 | LBL |

Table 3. continued.

| Source | RA.(J2000) | Dec.(J2000) | $\log v_{peak}$ | Class |
|--------------------|------------|-------------|-----------------|-------|
| MS 1050.7+4946 | 10:53:44.2 | 49:29:54 | 15.29 | IBL |
| FIRST J1054.5+3855 | 10:54:31.8 | 38:55:22 | 16.68 | HBL |
| RXS J1055.5-0126 | 10:55:34.1 | -01:26:05 | - | - |
| RXS J1056.1+0252 | 10:56:06.6 | 02:52:13 | - | - |
| FIRST J1057.3+2303 | 10:57:23.1 | 23:03:18 | 18.7 | HBL |
| RXS J1057.8+0059 | 10:57:52.4 | 00:59:13 | - | - |
| FIRST J1058.4+2817 | 10:58:29.9 | 28:17:46 | 18.37 | HBL |
| RXS J1058.6+5628 | 10:58:37.7 | 56:28:12 | 15.64 | IBL |
| MC 1057+100 | 11:00:20.2 | 09:49:35 | - | - |
| RXS J1100.3+4019 | 11:00:21.1 | 40:19:28 | 18.76 | HBL |
| RXS J1102.8-0148 | 11:02:52 | -01:48:51 | - | - |
| MRK 421 | 11:04:27.2 | 38:12:32 | 18.49 | HBL |
| 1ES 1106+244 | 11:09:16.2 | 24:11:20 | 16.91 | HBL |
| OP 1106.7+3654 | 11:09:33.5 | 36:38:26 | - | - |
| FIRST J1110.9+3539 | 11:10:56.9 | 35:39:06 | - | - |
| RXS J1110.6+7133 | 11:10:37.5 | 71:33:57 | 16.96 | HBL |
| RXS J1111.5+3452 | 11:11:30.9 | 34:52:00 | - | - |
| FIRST J1117.6+2548 | 11:17:40.4 | 25:48:46 | 15.71 | IBL |
| EXO 1118.0+4228 | 11:20:48.1 | 42:12:13 | 17.41 | HBL |
| US 2504 | 11:29:50.1 | 26:52:53 | 12.97 | LBL |
| MS 1133.7+1618 | 11:36:17.6 | 16:01:53 | 15.9 | IBL |
| MRK 180 | 11:36:26.5 | 70:09:28 | 18.61 | HBL |
| RXS J1136.5+6737 | 11:36:30.1 | 67:37:04 | 17.55 | HBL |
| FIRST J1136.8+2550 | 11:36:50.1 | 25:50:52 | 15.13 | IBL |
| 2E 1146+2456 | 11:49:29.9 | 24:38:55 | 17.87 | HBL |
| EXO 1449.9+2455 | 11:49:30.3 | 24:39:27 | 19.83 | HBL |
| B2 1147+245 | 11:50:19.2 | 24:17:54 | 13.95 | LBL |
| RXS J1151.4+5859 | 11:51:24.6 | 58:59:14 | 16.4 | IBL |
| FIRST J1152.1+2837 | 11:52:10.7 | 28:37:21 | 14.8 | IBL |
| FIRST J1153.7+3823 | 11:53:42.9 | 38:23:06 | - | - |
| MS 1154.1+4255 | 11:56:46.6 | 42:38:10 | 14.91 | IBL |
| B3 1159+450 | 12:02:08.6 | 44:44:21 | 15.92 | IBL |
| B3 1206+416 | 12:09:22.8 | 41:19:41 | 14.59 | IBL |
| 1207+39W4 | 12:10:26.6 | 39:29:08 | - | - |
| MS 1209.0+3917 | 12:11:34.2 | 39:00:55 | - | - |
| 1ES 1212+078 | 12:15:10.9 | 07:32:03 | 15.91 | IBL |
| Q 1214+1753 | 12:16:56.9 | 17:37:12 | - | - |
| B2 1215+30 | 12:17:52 | 30:07:01 | 15.58 | IBL |
| GB2 1217+348 | 12:20:08.4 | 34:31:22 | 14.46 | LBL |
| PG 1218+304 | 12:21:21.9 | 30:10:37 | 19.14 | HBL |
| ON 231 | 12:21:31.7 | 28:13:58 | 14.84 | IBL |
| UM 493 | 12:22:06.5 | -01:06:38 | - | - |
| RXS J1222.2+3541 | 12:22:12.4 | 35:41:00 | 12.81 | LBL |
| S5 1221+80 | 12:23:40.4 | 80:40:04 | 14.21 | LBL |
| MS 1221.8+2452 | 12:24:24.3 | 24:36:24 | 13.99 | LBL |
| 1WGA J1225.3+1818 | 12:25:18.2 | 18:18:20 | 14.71 | IBL |
| FIRST J1226.0+2604 | 12:26:04.1 | 26:04:28 | 16.29 | IBL |
| RXS J1230.2+2517 | 12:30:14 | 25:18:06 | 14.9 | IBL |
| 2E 1258+1437 | 12:31:23.9 | 14:21:25 | 14.91 | IBL |
| MS 1229.2+6430 | 12:31:31.3 | 64:14:18 | 16.25 | IBL |
| B2 1229+29 | 12:31:43.6 | 28:47:49 | - | - |
| FIRST J1236.3+3900 | 12:36:23.1 | 39:00:01 | 16.61 | HBL |
| MS 1235.4+6315 | 12:37:38.6 | 62:58:44 | 15.98 | IBL |
| RXS J1237.0+3020 | 12:37:05.5 | 30:20:04 | - | - |

Table 3. continued.

| Source | RA.(J2000) | Dec.(J2000) | $\log v_{peak}$ | Class |
|--------------------|-------------|-------------|-----------------|-------|
| 1ES 1239+069 | 12:41:48.3 | 06:36:01 | 17.38 | HBL |
| RXS J1241.6+3440 | 12:41:41.2 | 34:40:32 | - | - |
| Ton 116 | 12:43:12.7 | 36:27:44 | - | - |
| PG 1246+586 | 12:48:18.8 | 58:20:29 | 15.05 | IBL |
| 1ES 1249+174E | 12:51:45.5 | 17:11:17 | - | - |
| FIRST J1252.3+2640 | 12:52:19.5 | 26:40:53 | - | - |
| S4 1250+53 | 12:53:11.9 | 53:01:11 | 14.82 | IBL |
| 1ES 1255+244 | 12:57:31.9 | 24:12:40 | 16.89 | HBL |
| MS 1256.3+0151 | 12:58:54.6 | 01:34:43 | - | - |
| MS 1258.4+6401 | 13:00:17.6 | 63:44:39 | 16.35 | IBL |
| FIRST J1301.7+4056 | 13:01:45.7 | 40:56:24 | 16.55 | HBL |
| RXS J1302.9+5056 | 13:02:55.5 | 50:56:17 | - | - |
| MC2 1307+12 | 13:09:33.9 | 11:54:24 | 13.07 | LBL |
| 1WGA J1309.6+0828 | 13:09:38.9 | 08:28:28 | 14.64 | IBL |
| AUCVn | 13:10:28.66 | 32:30:43.8 | 13.75 | LBL |
| HS 1309+2605 | 13:12:19.2 | 25:49:58 | - | - |
| TEX 1312+240 | 13:14:43.8 | 23:48:26 | 15.84 | IBL |
| RXS J1319.5+1405 | 13:19:31.7 | 14:05:34 | 20.85 | HBL |
| UM 566 | 13:19:55.1 | 01:52:58 | - | - |
| 1ES 1320+084N | 13:22:54.9 | 08:10:10 | 13.12 | LBL |
| RXS J1324.0+5739 | 13:24:00.8 | 57:39:16 | 15.48 | IBL |
| RXS J1326.2+2933 | 13:26:15 | 29:33:29 | - | - |
| RXS J1326.2+1230 | 13:26:17.6 | 12:30:00 | 16.32 | IBL |
| RX J1340.1+2743 | 13:40:10.9 | 27:43:48 | - | - |
| RXS J1340.4+4410 | 13:40:29.8 | 44:10:04 | 16.51 | HBL |
| RXS J1341.0+3959 | 13:41:05 | 39:59:45 | 20.06 | HBL |
| 1338.8+2705 | 13:41:05.8 | 26:50:26 | - | - |
| 1340.8+2721 | 13:43:05.1 | 27:06:24 | - | - |
| RXS J1353.4+5601 | 13:53:28 | 56:00:55 | 19.23 | HBL |
| FIRST J1354.4+3706 | 13:54:26.7 | 37:06:54 | 16.92 | HBL |
| RXS J1359.8+5911 | 13:59:53.7 | 59:11:01 | 13.66 | LBL |
| MC 1400+162 | 14:02:44.5 | 15:59:57 | 16.47 | IBL |
| RXS J1404.8+6554 | 14:04:49.6 | 65:54:30 | - | - |
| MS 1402.3+0416 | 14:04:51 | 04:02:02 | 15.83 | IBL |
| MS 1407.9+5954 | 14:09:23.5 | 59:39:41 | 16.63 | HBL |
| PKS 1407+022 | 14:10:04.6 | 02:03:07 | 13.69 | LBL |
| RXS J1410.5+6100 | 14:10:31.7 | 61:00:10 | 20.25 | HBL |
| FIRST J1414.1+3430 | 14:14:09.3 | 34:30:57 | - | - |
| RGB J1415+485 | 14:15:36.8 | 48:30:30 | 14.56 | IBL |
| PKS 1413+135 | 14:15:58.8 | 13:20:24 | 12.83 | LBL |
| CRSS 1416.3+1137 | 14:16:20.7 | 11:37:37 | - | - |
| 2E 1415+2557 | 14:17:56.6 | 25:43:25 | 19.24 | HBL |
| OQ 530 | 14:19:46.6 | 54:23:14 | 14.16 | LBL |
| RXS J1422.6+5801 | 14:22:39 | 58:01:55 | - | - |
| FIRST J1426.1+3404 | 14:26:07.7 | 34:04:26 | 14.1 | LBL |
| PKS 1424+240 | 14:27:00.5 | 23:48:00 | 15.7 | IBL |
| RGB J1427+541 | 14:27:30.3 | 54:09:24 | 14.89 | IBL |
| H 1426+428 | 14:28:32.7 | 42:40:21 | 18.55 | HBL |
| TEX 1428+370 | 14:30:40.6 | 36:49:03 | 14.26 | LBL |
| CSO 474 | 14:36:45.7 | 35:57:01 | - | - |
| RXS J1436.9+5639 | 14:36:57.8 | 56:39:25 | 17.5 | HBL |
| PG 1437+398 | 14:39:17.5 | 39:32:43 | 16.7 | HBL |
| 1ES 1440+122 | 14:42:48.3 | 12:00:40 | 16.45 | IBL |
| MS 1443.5+6349 | 14:44:34.9 | 63:36:06 | 17.05 | HBL |

Table 3. continued.

| Source | RA.(J2000) | Dec.(J2000) | $\log v_{peak}$ | Class |
|--------------------|------------|-------------|-----------------|-------|
| RXS J1445.0-0326 | 14:45:06.2 | -03:26:12 | - | - |
| RXS J1448.0+3608 | 14:48:00.6 | 36:08:31 | 16.73 | HBL |
| RXS J1449.5+2746 | 14:49:32.8 | 27:46:21 | 18.82 | HBL |
| RXS J1451.4+6354 | 14:51:27.5 | 63:54:19 | - | - |
| SBS 1452+516 | 14:54:27.1 | 51:24:33 | - | - |
| RXS J1456.0+5048 | 14:56:03.7 | 50:48:25 | 19.94 | HBL |
| RXS J1458.4+4832 | 14:58:28 | 48:32:40 | 21.46 | HBL |
| B3 1456+375 | 14:58:44.8 | 37:20:22 | 13.47 | LBL |
| MS 1458.8+2249 | 15:01:01.9 | 22:38:06 | 15.26 | IBL |
| FIRST J1502.1+2528 | 15:02:08.3 | 25:28:45 | 14.17 | LBL |
| FIRST J1502.5+3350 | 15:02:34 | 33:50:55 | 13.66 | LBL |
| RXS J1508.7+2709 | 15:08:42.9 | 27:09:10 | 17.3 | HBL |
| SBS 1508+561 | 15:09:48 | 55:56:17 | 15.22 | IBL |
| FIRST J1515.9+2426 | 15:15:56.2 | 24:26:20 | 15.89 | IBL |
| RXS J1516.7+2918 | 15:16:41.6 | 29:18:10 | 18.62 | HBL |
| PKS 1514+197 | 15:16:56.8 | 19:32:12 | 13.6 | LBL |
| 1H 1515+660 | 15:17:47.6 | 65:25:24 | 18.11 | HBL |
| FIRST J1530.7+2310 | 15:30:44 | 23:10:13 | - | - |
| FAQS J1530.7+5329 | 15:30:44.5 | 53:29:28 | 16.88 | HBL |
| RXS J1532.0+3016 | 15:32:02.2 | 30:16:29 | 17.05 | HBL |
| RXS J1533.4+3416 | 15:33:24.3 | 34:16:41 | 18.32 | HBL |
| RGB J1534+372 | 15:34:47.2 | 37:15:55 | 14.26 | LBL |
| 1ES 1533+535 | 15:35:00.8 | 53:20:37 | 19.68 | HBL |
| FIRST J1535.4+3922 | 15:35:29.1 | 39:22:46 | 16.38 | IBL |
| MS 1534.2+0148 | 15:36:46.8 | 01:37:59 | 18.83 | HBL |
| 1ES 1544+820 | 15:40:15.8 | 81:55:07 | 17.79 | HBL |
| 4C 14.6 | 15:40:46.5 | 14:47:45.9 | 14.85 | IBL |
| RXS J1542.9+6129 | 15:42:56.9 | 61:29:56 | 14.72 | IBL |
| RXS J1544.3+0458 | 15:44:18.7 | 04:58:24 | 16.77 | HBL |
| MS 1552.1+2020 | 15:54:24.1 | 20:11:25 | 17.12 | HBL |
| PG 1553+11 | 15:55:43.1 | 11:11:24 | 16.49 | IBL |
| MYC 1557+566 | 15:58:48.5 | 56:25:14 | - | - |
| RXS J1602.2+3050 | 16:02:18 | 30:51:09 | 16.42 | IBL |
| PKS 1604+159 | 16:07:06.4 | 15:51:34 | 14.73 | IBL |
| RXS J1610.0+6710 | 16:10:04.1 | 67:10:26 | 17.45 | HBL |
| B3 1615+412 | 16:17:06.6 | 41:06:45 | 14.41 | LBL |
| 87GB 16166+2206 | 16:18:47.9 | 21:59:26 | 15.66 | IBL |
| 4C 37.46 | 16:21:11.3 | 37:46:04.9 | - | - |
| RXJ 1624.7+3726 | 16:24:43.4 | 37:26:42 | - | - |
| RXS J1624.9+7554 | 16:24:56.5 | 75:54:55 | 13.3 | LBL |
| RXS J1626.4+3513 | 16:26:25.6 | 35:13:38 | 15.28 | IBL |
| RXS J1631.3+4217 | 16:31:24.7 | 42:17:03 | 18.99 | HBL |
| RXS J1638.0+7326 | 16:38:02.6 | 73:26:10 | - | - |
| RXS J1644.2+4546 | 16:44:20 | 45:46:44 | 17.48 | HBL |
| 1643.2+4021 | 16:44:53.2 | 40:16:28 | - | - |
| FIRST J1645.9+2947 | 16:45:57.7 | 29:47:30 | - | - |
| FIRST J1651.1+4212 | 16:51:09.2 | 42:12:53 | 17.82 | HBL |
| RXS J1651.6+7218 | 16:51:41.5 | 72:18:19 | - | - |
| RGB J1652+403 | 16:52:50 | 40:23:10 | 14.97 | IBL |
| MRK 501 | 16:53:52.2 | 39:45:36 | 16.84 | HBL |
| B3 1659+399 | 17:01:24.6 | 39:54:36 | 13.41 | LBL |
| FIRST J1702.1+2643 | 17:02:09.6 | 26:43:15 | 14.27 | LBL |
| FIRST J1702.6+3115 | 17:02:38.6 | 31:15:43 | 13.49 | LBL |
| RXS J1704.8+7138 | 17:04:46.9 | 71:38:18 | 15.58 | IBL |

Table 3. continued.

| Source | RA.(J2000) | Dec.(J2000) | $\log v_{peak}$ | Class |
|--------------------|-------------|-------------|-----------------|-------|
| MS 1704.9+6046 | 17:05:34.9 | 60:42:17 | 17.17 | HBL |
| FIRST J1712.8+2931 | 17:12:48.8 | 29:31:17 | 18.79 | HBL |
| RXS J1718.6+7358 | 17:18:40.1 | 73:58:15 | - | - |
| PKS 1717+177 | 17:19:13.1 | 17:45:07 | 13.08 | LBL |
| RXS J1719.6+7443 | 17:19:41 | 74:43:00 | 14.19 | LBL |
| B2 1722+40 | 17:24:05.5 | 40:04:38 | 13 | LBL |
| H 1722+119 | 17:25:04.4 | 11:52:16 | 15.8 | IBL |
| IZw187 | 17:28:18.6 | 50:13:11 | 17.42 | HBL |
| RXS J1728.6+7041 | 17:28:38.3 | 70:41:08 | 13.6 | LBL |
| RXS J1732.0+6926 | 17:32:05.4 | 69:26:16 | - | - |
| OT 465 | 17:39:57.1 | 47:37:59 | 13.91 | LBL |
| RGBJ 1742+597 | 17:42:32 | 59:45:06 | 14.18 | LBL |
| NPM1G +19.0510 | 17:43:57.9 | 19:35:09 | 17.91 | HBL |
| B3 1743+398B | 17:45:37.7 | 39:51:31 | 17.71 | HBL |
| 1ES 1745+504 | 17:46:32.3 | 50:28:09 | - | - |
| B3 1746+470 | 17:47:26.6 | 46:58:51 | 13.96 | LBL |
| S4 1749+70 | 17:48:33.1 | 70:05:50 | 14.55 | IBL |
| B3 1747+433 | 17:49:00.4 | 43:21:52 | 13.56 | LBL |
| RXS J1750.0+4700 | 17:50:05 | 47:00:44 | 18.1 | HBL |
| PKS 1749+096 | 17:51:32.7 | 09:39:01 | 12.78 | LBL |
| RXS J1756.2+5522 | 17:56:15.9 | 55:22:18 | 19.9 | HBL |
| MS 1757.7+7034 | 17:57:13.3 | 70:33:37 | 13.7 | LBL |
| S5 1803+784 | 18:00:45.4 | 78:28:04 | 14.05 | LBL |
| RX J1801.7+6638 | 18:01:46.7 | 66:38:40 | - | - |
| 3C 371 | 18:06:50.7 | 69:49:28 | 14.65 | IBL |
| RGB J1808+468 | 18:08:01.2 | 46:49:41 | 14.63 | IBL |
| RGB J1811+442 | 18:11:53.5 | 44:16:29 | 15.07 | IBL |
| B2 1811+31 | 18:13:35.3 | 31:44:17 | 15.53 | IBL |
| 4C 56.27 | 18:24:07.07 | 56:51:01.5 | 12.95 | LBL |
| RXS J1829.4+5402 | 18:29:24.3 | 54:03:00 | 15.07 | IBL |
| Q 1832+6845 | 18:32:36.6 | 68:48:09 | - | - |
| RXS J1838.7+4802 | 18:38:49.2 | 48:02:34 | 13.52 | LBL |
| RGB J1841+591 | 18:41:20.3 | 59:06:08 | 14.91 | IBL |
| RXS J1848.7+4245 | 18:48:47.1 | 42:45:39 | - | - |
| 1ES 1853+671 | 18:53:52.1 | 67:13:55 | 16.64 | HBL |
| 87GB 19021+5536 | 19:03:11.6 | 55:40:39 | 14.5 | LBL |
| S4 1926+61 | 19:27:30.4 | 61:17:32 | 13.44 | LBL |
| RXS J1931.1+0937 | 19:31:09.5 | 09:37:13 | - | - |
| 1ES 1959+650 | 19:59:59.9 | 65:08:55 | 18.03 | HBL |
| S5 2007+77 | 20:05:31.1 | 77:52:43 | 13.15 | LBL |
| S5 2010+72 | 20:09:52.3 | 72:29:19 | 13.64 | LBL |
| PKS 2012-017 | 20:15:15.1 | -01:37:33 | 14.68 | IBL |
| S5 2023+76 | 20:22:35.6 | 76:11:26 | 14.1 | LBL |
| PKS 2032+107 | 20:35:22.3 | 10:56:06 | 14 | LBL |
| 1ES 2037+521 | 20:39:23.5 | 52:19:50 | 16.13 | IBL |
| PKS 2047+039 | 20:50:06.2 | 04:07:49 | 13.83 | LBL |
| S5 2051+74 | 20:51:33.8 | 74:41:40 | 18.75 | HBL |
| PKS 2131-021 | 21:34:10.2 | -01:53:17 | 12.76 | LBL |
| MS 2143.4+0704 | 21:45:52.3 | 07:19:27 | 13.92 | LBL |
| PKS 2149+17 | 21:52:24.8 | 17:34:39 | 13.85 | LBL |
| BL LAC | 22:02:43.3 | 42:16:39 | 14.28 | LBL |
| RXS J2209.3+1031 | 22:09:18.5 | 10:31:43 | 13.36 | LBL |
| RXS J2219.7+2120 | 22:19:45.3 | 21:20:48 | 17.61 | HBL |
| RXS J2225.1+1136 | 22:25:11.2 | 11:36:01 | - | - |

Table 3. continued.

| Source | RA.(J2000) | Dec.(J2000) | $\log \nu_{peak}$ | Class |
|------------------|------------|-------------|-------------------|-------|
| PKS 2223-114 | 22:25:43.7 | -11:13:41 | 14.65 | IBL |
| 3C 446 | 22:25:45.1 | -04:56:34 | 13.37 | LBL |
| S5 2229+69 | 22:30:35.6 | 69:46:29 | 13.09 | LBL |
| RXS J2233.0+1335 | 22:33:00.9 | 13:35:59 | 16.61 | HBL |
| RGB J2243+203 | 22:43:54.7 | 20:21:04 | 14.15 | LBL |
| B3 2247+381 | 22:50:05.8 | 38:24:37 | 15.61 | IBL |
| PKS 2254+074 | 22:57:17.3 | 07:43:12 | 14.18 | LBL |
| RXS J2304.6+3705 | 23:04:36.6 | 37:05:08 | 21.01 | HBL |
| B3 2311+396A | 23:13:50.2 | 40:03:03 | - | - |
| Q J2319+161 | 23:19:43.4 | 16:11:51 | 15.48 | IBL |
| TEX 2320+343 | 23:22:44 | 34:36:14 | 16.73 | HBL |
| 1ES 2321+419 | 23:23:54.1 | 42:11:19 | 13.26 | LBL |
| B3 2322+396 | 23:25:17.9 | 39:57:37 | 15.29 | IBL |
| 1ES 2326+174 | 23:29:03.3 | 17:43:30 | 18.07 | HBL |
| Q J2338+212 | 23:38:56.4 | 21:24:41 | 17.62 | HBL |
| MS 2336.5+0517 | 23:39:07 | 05:34:36 | 14.91 | IBL |
| 1ES 2344+514 | 23:47:04.8 | 51:42:18 | 16.4 | IBL |
| MS 2347.4+1924 | 23:50:01.7 | 19:41:52 | 15.8 | IBL |
| RXS J2350.3-059 | 23:50:17.9 | -05:59:28 | - | - |
| TEX 2348+360 | 23:50:36.7 | 36:22:11 | 16.1 | IBL |
| PKS 2354-02 | 23:57:25.1 | -01:52:15 | - | - |

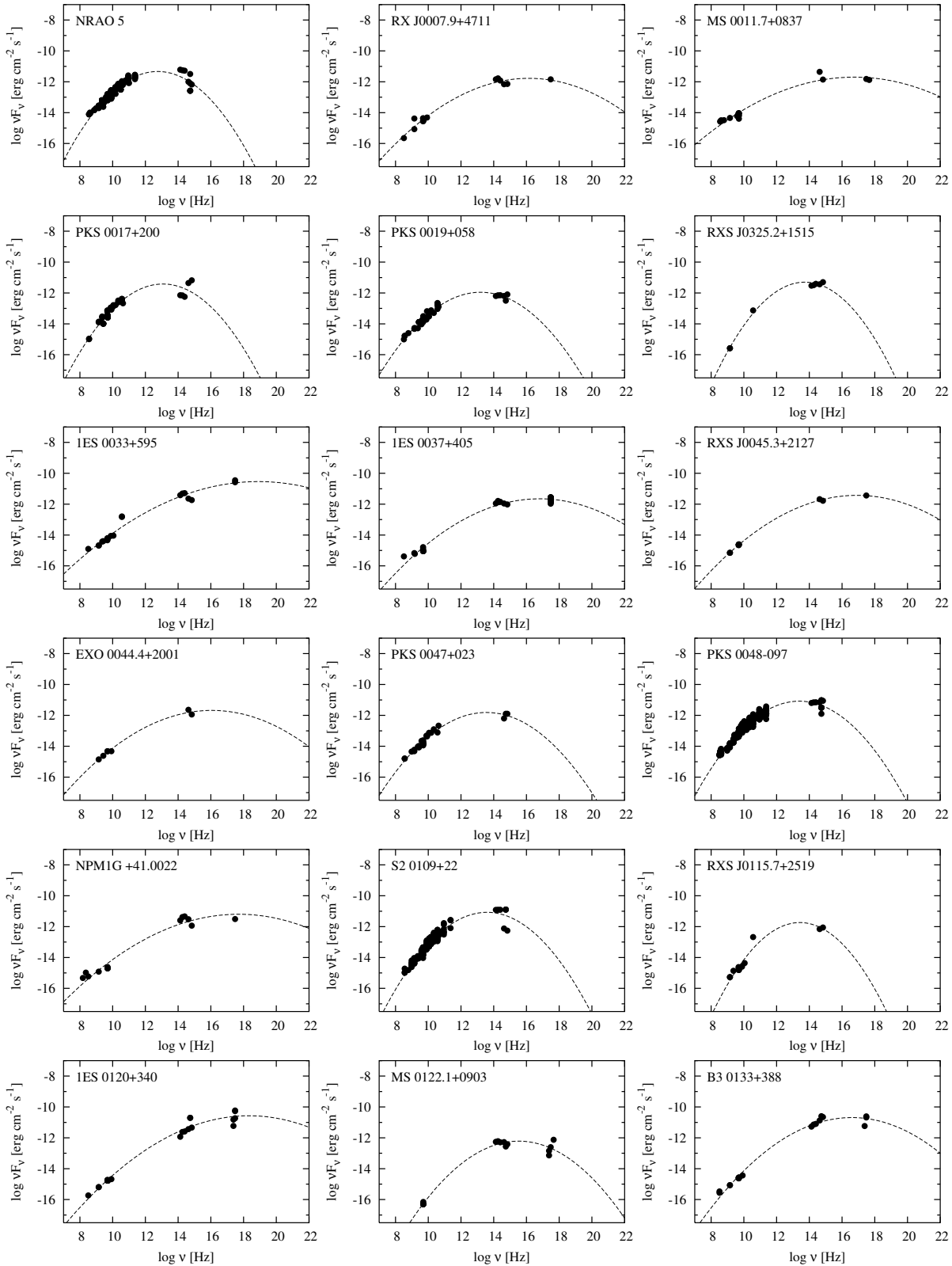


Fig. 13. Spectral energy distributions of the Metsähovi BL Lac sample. Only datapoints used in the fit are shown in the figure.

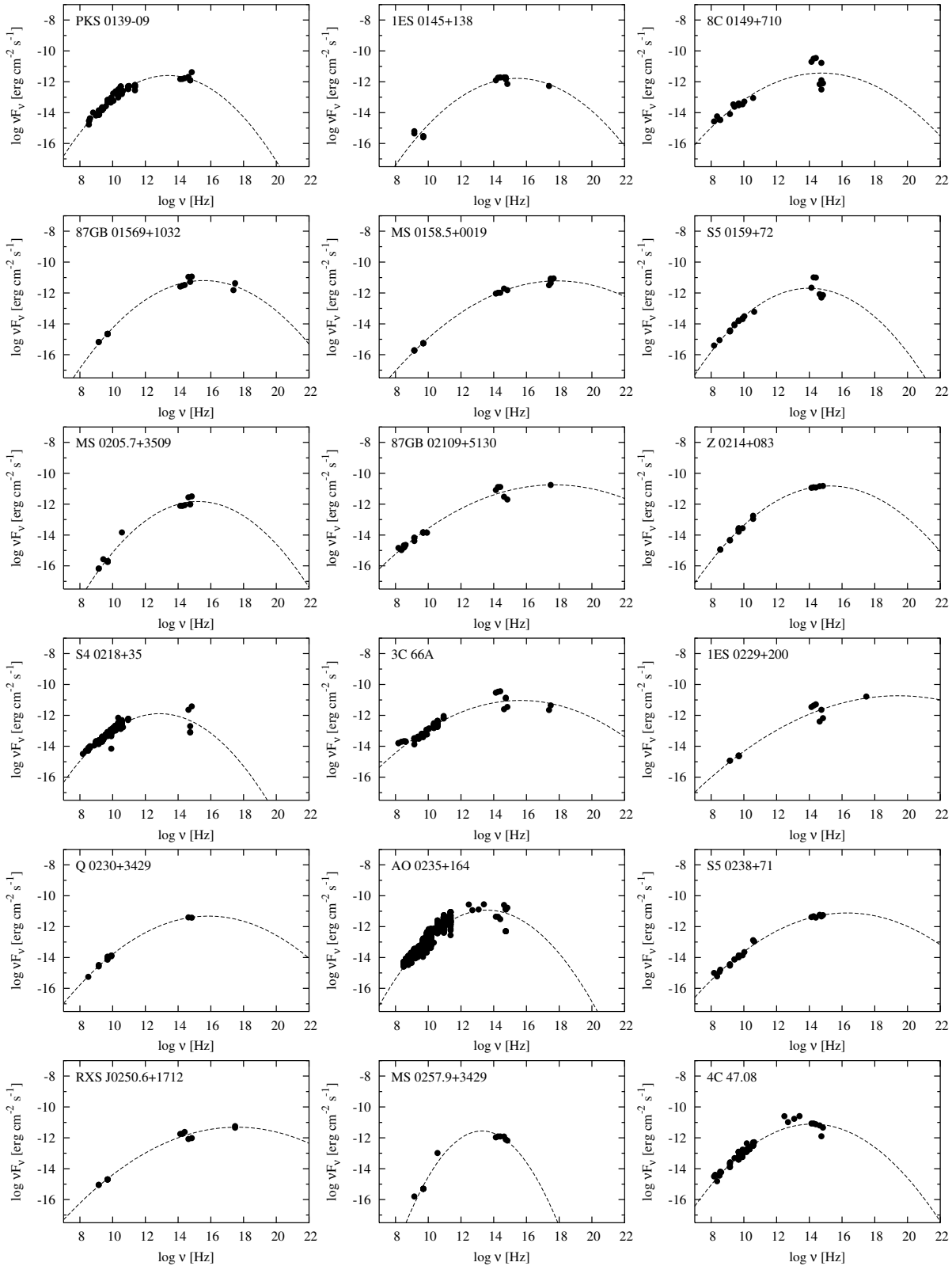


Fig. 13. continued.

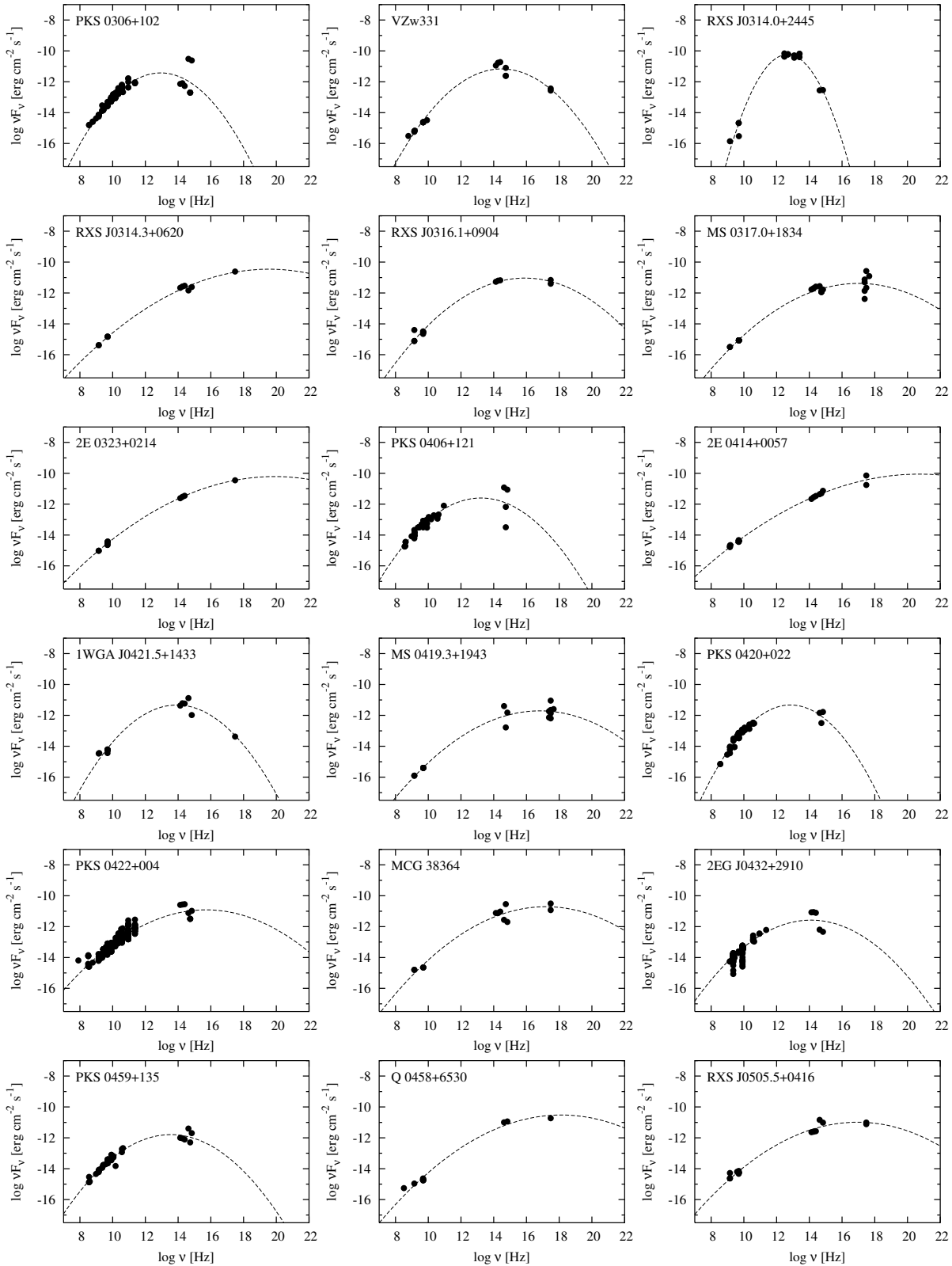


Fig. 13. continued.

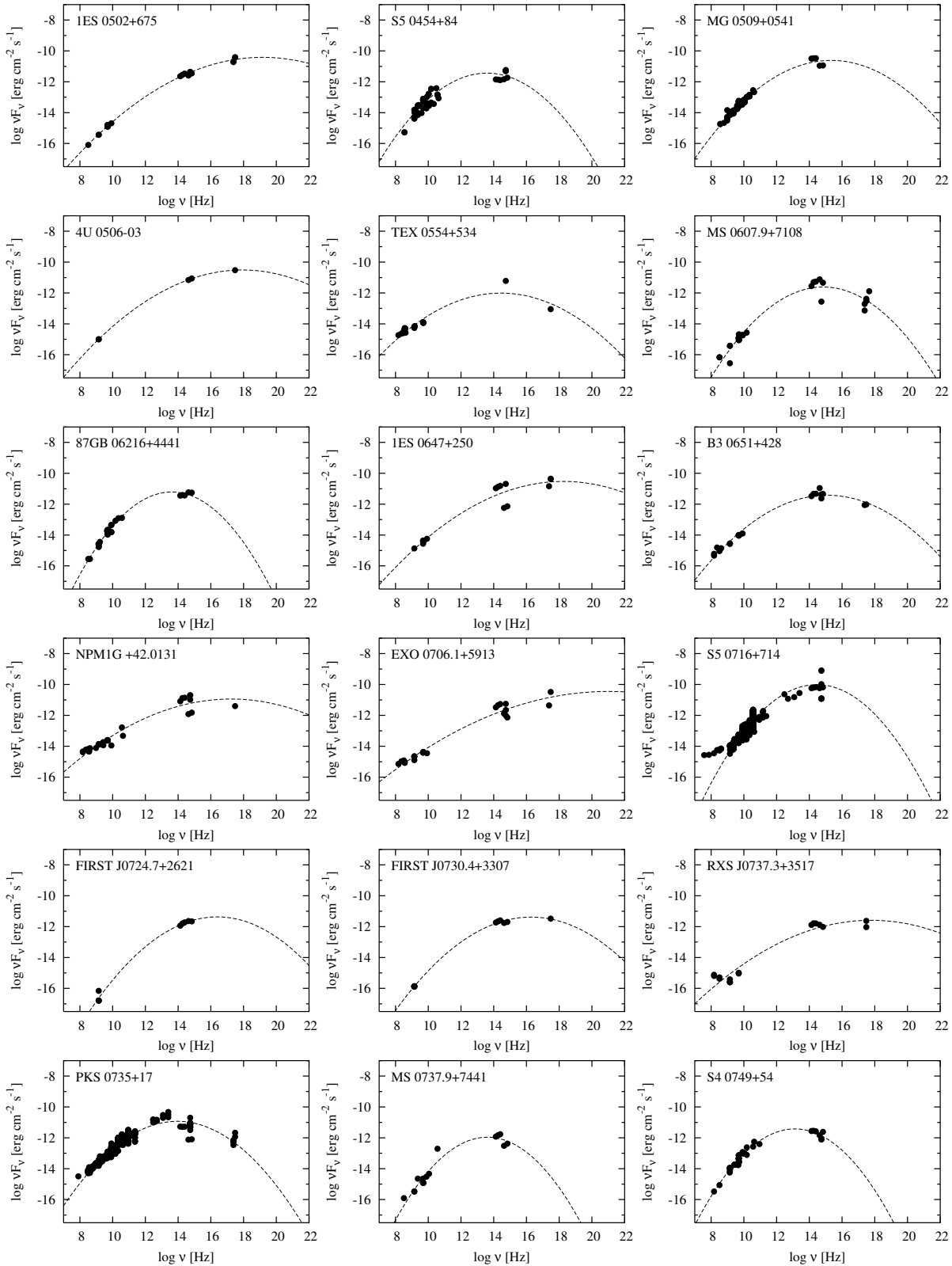


Fig. 13. continued.

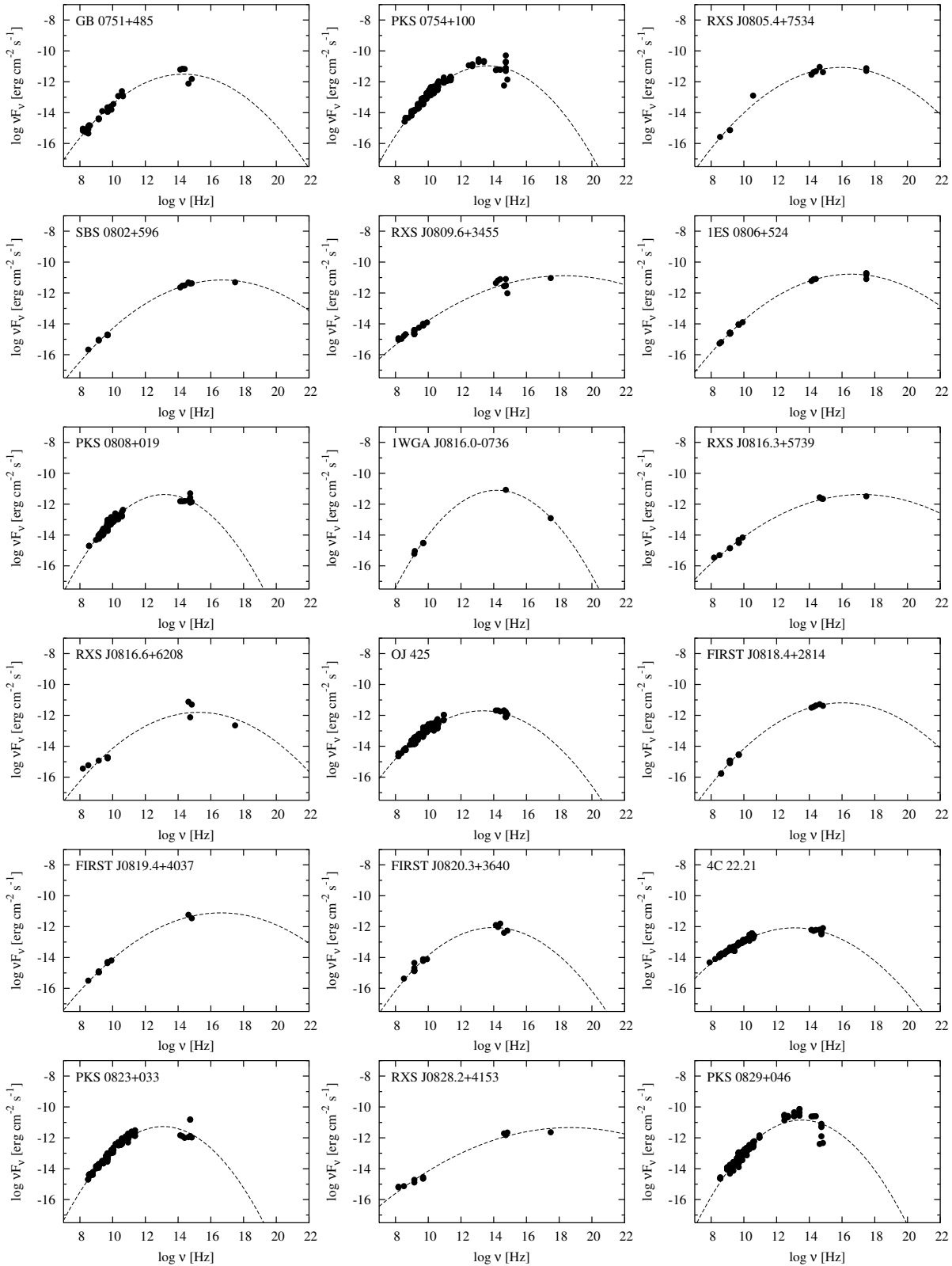


Fig. 13. continued.

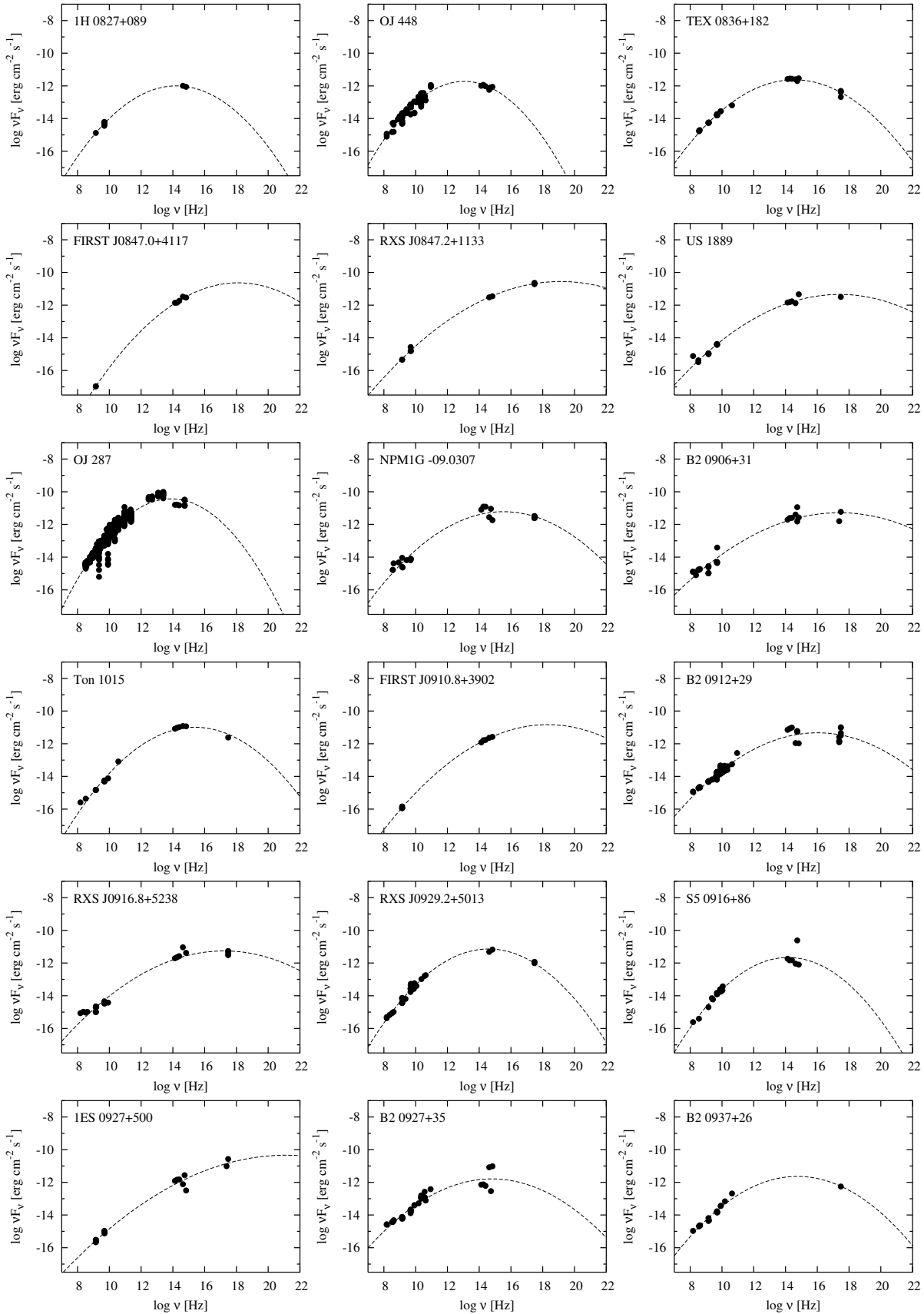


Fig. 13. continued.

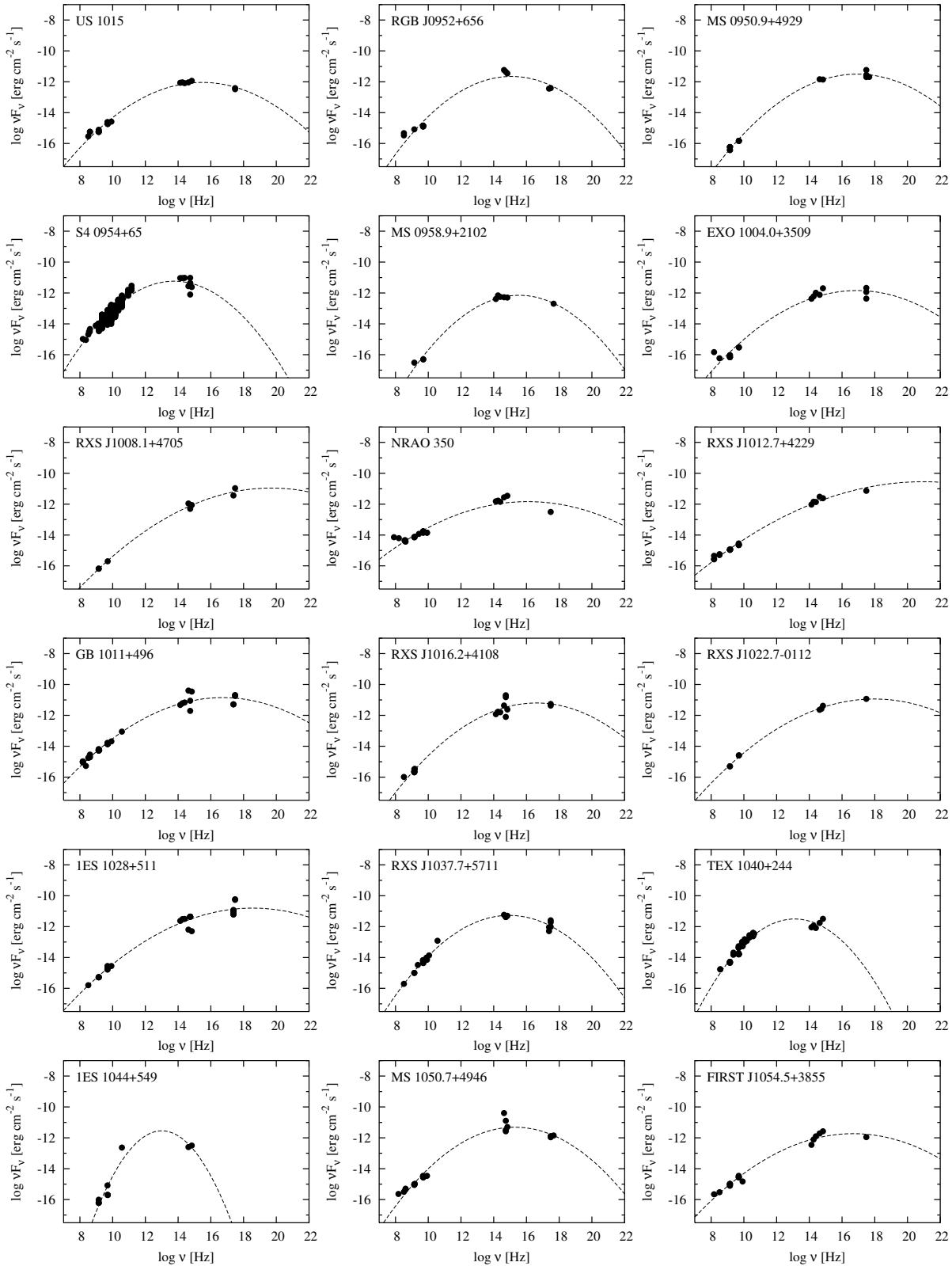


Fig. 13. continued.

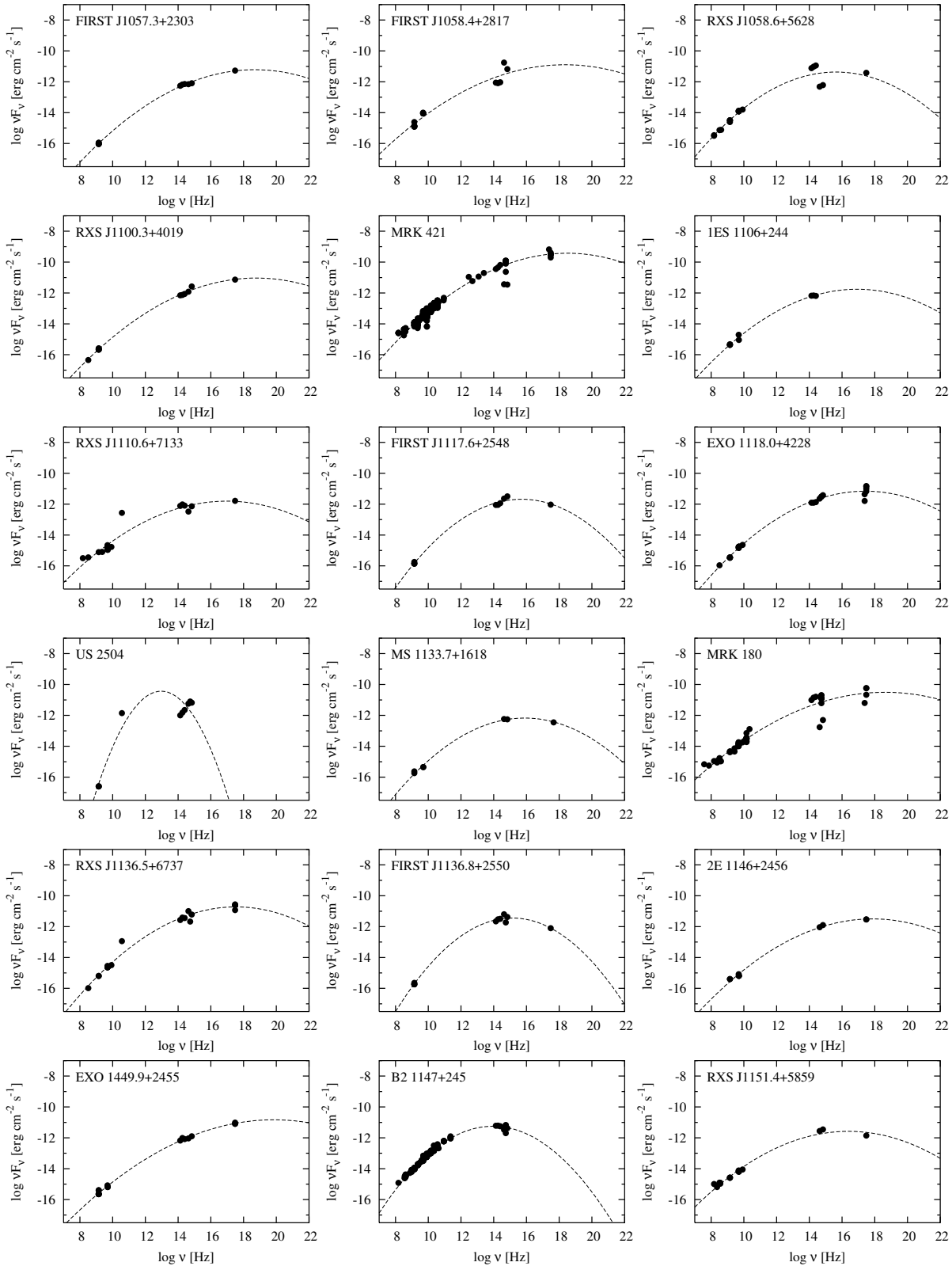


Fig. 13. continued.

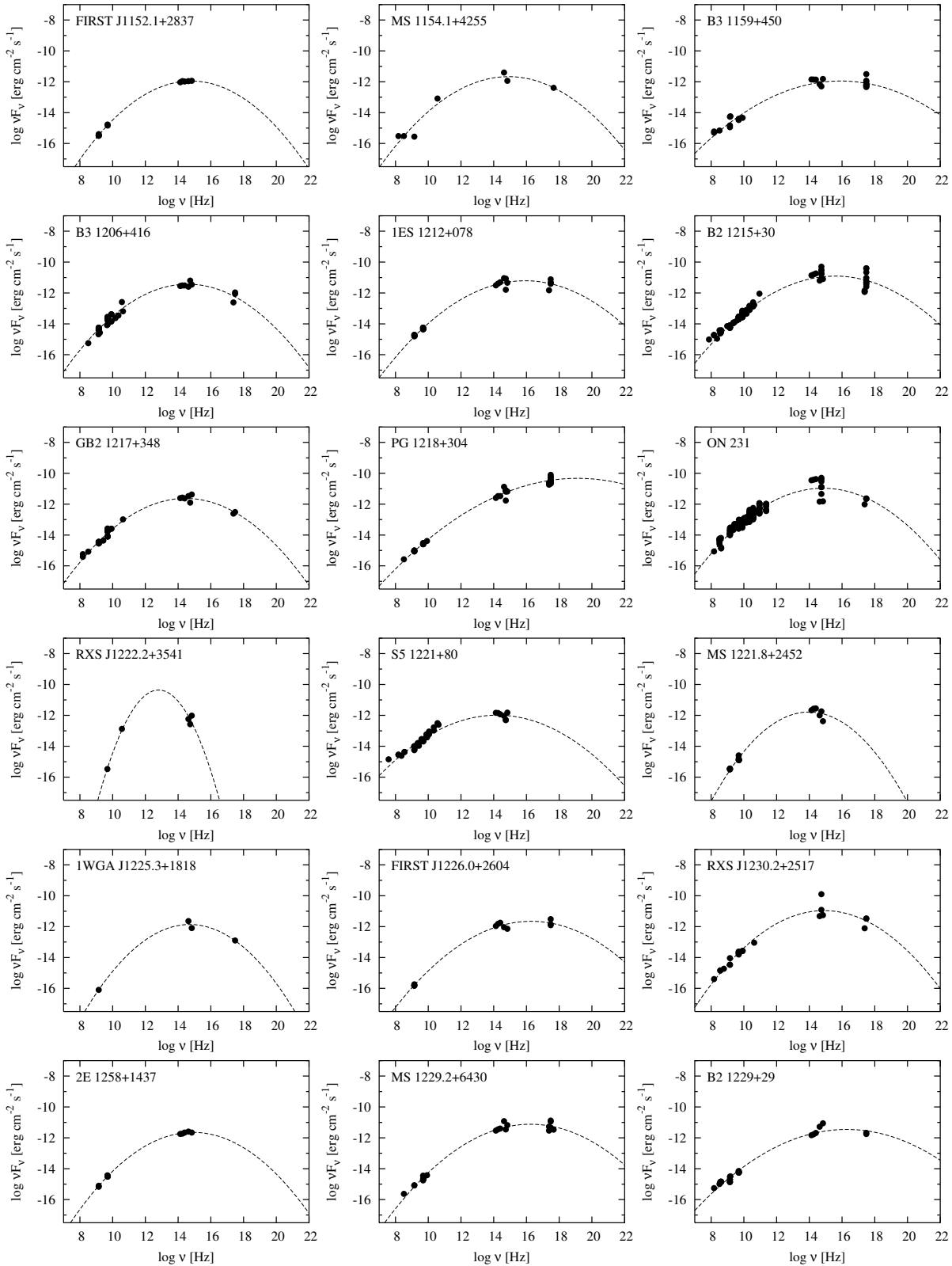


Fig. 13. continued.

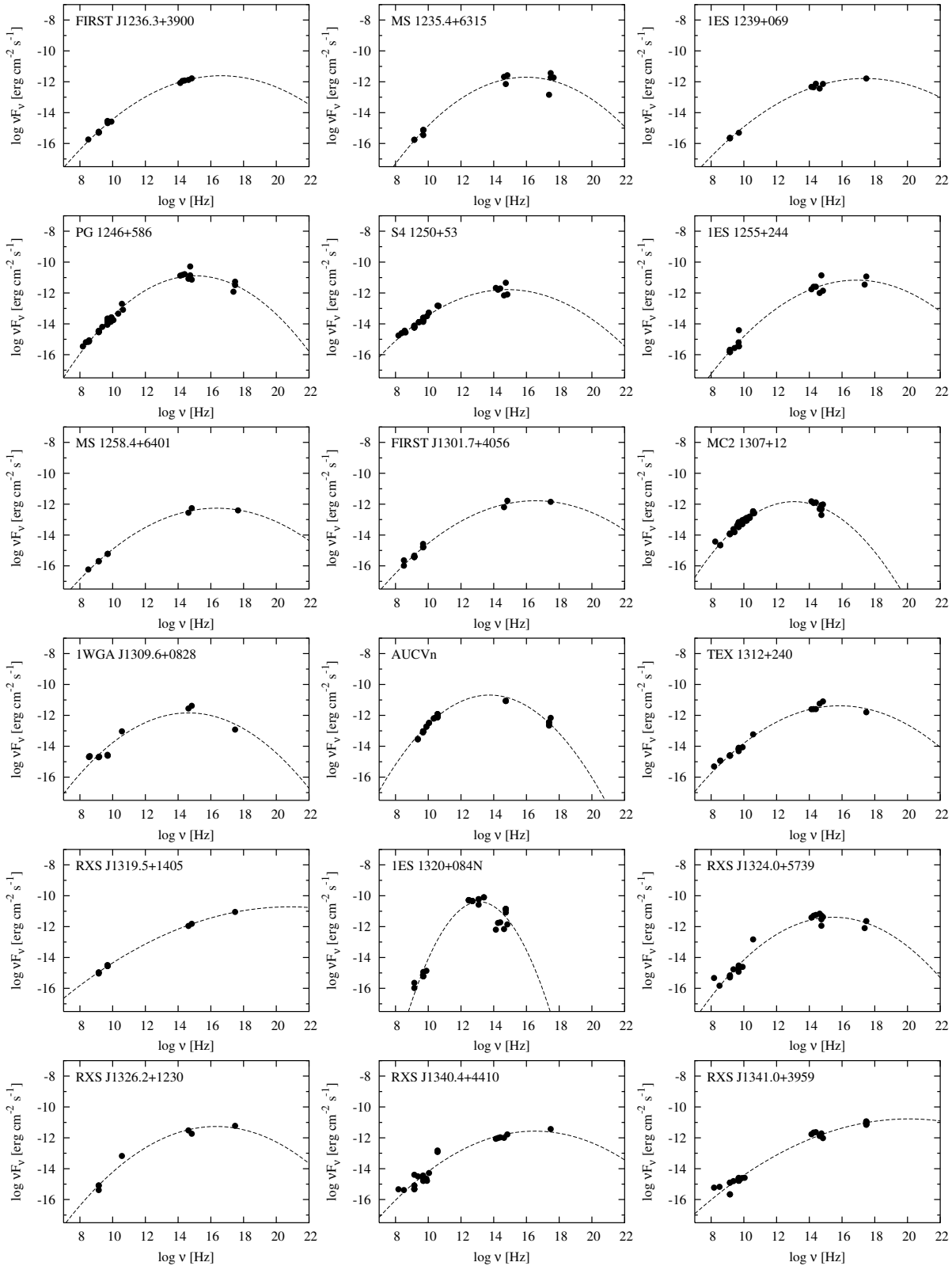


Fig. 13. continued.

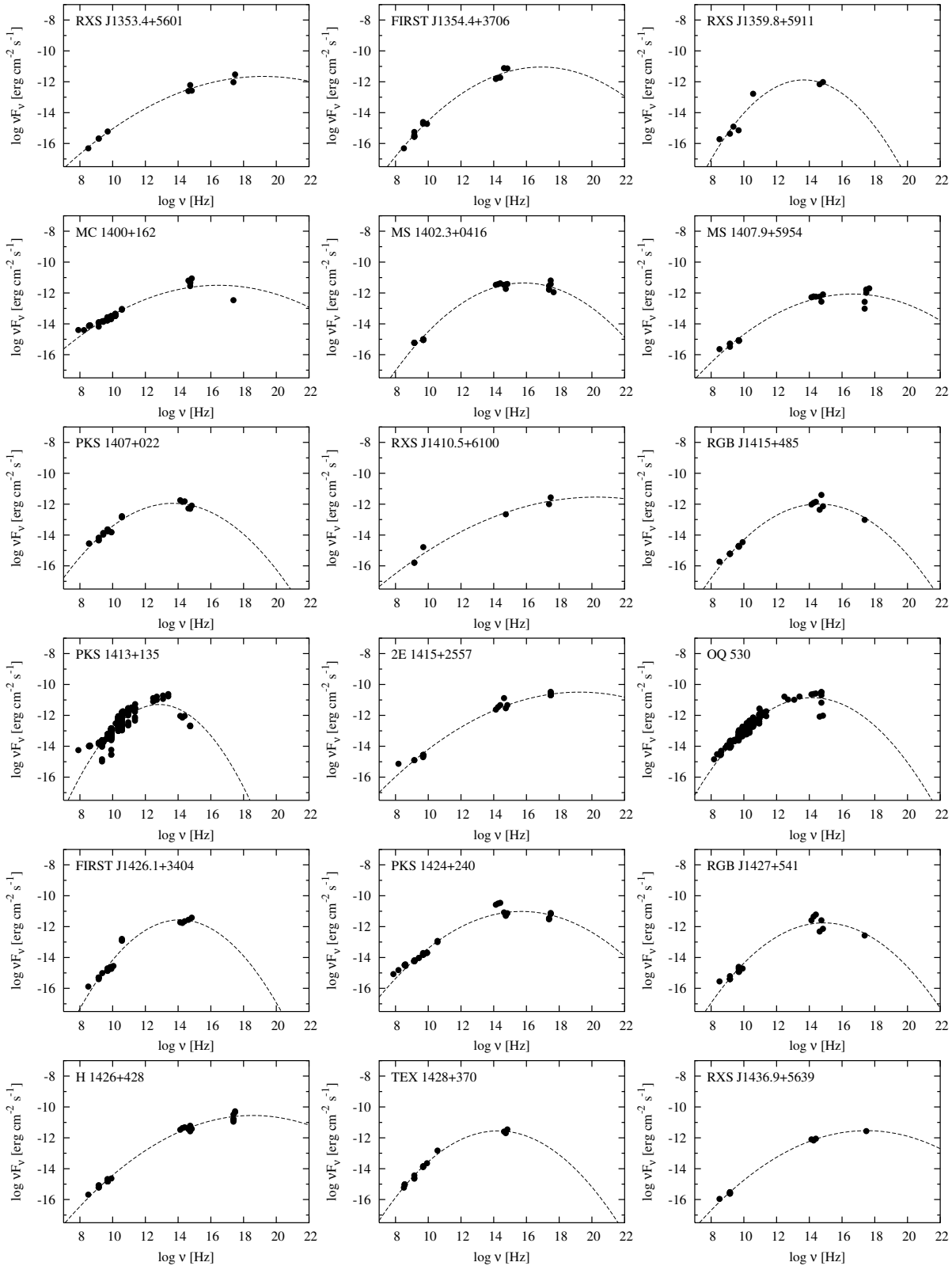


Fig. 13. continued.

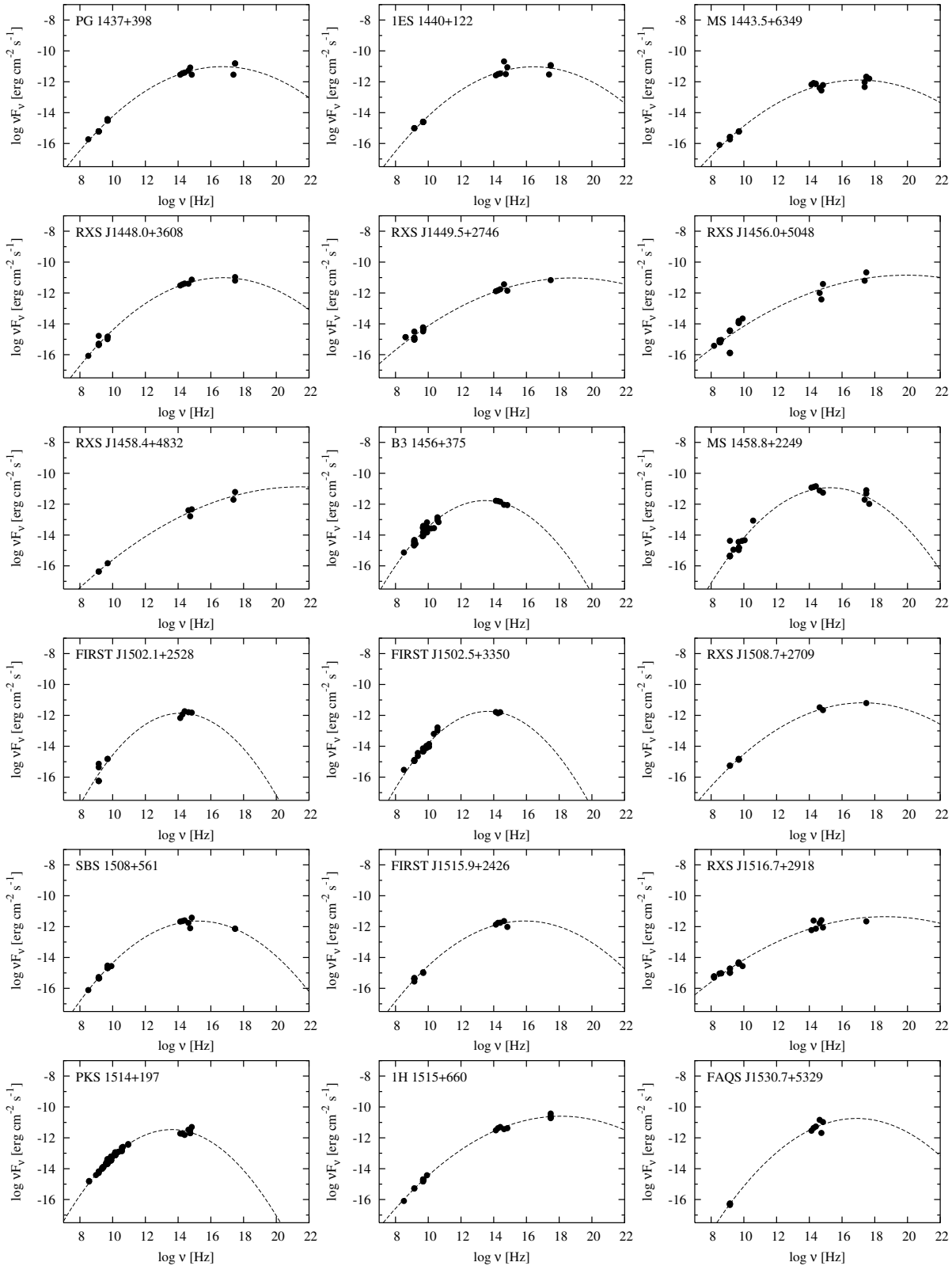


Fig. 13. continued.

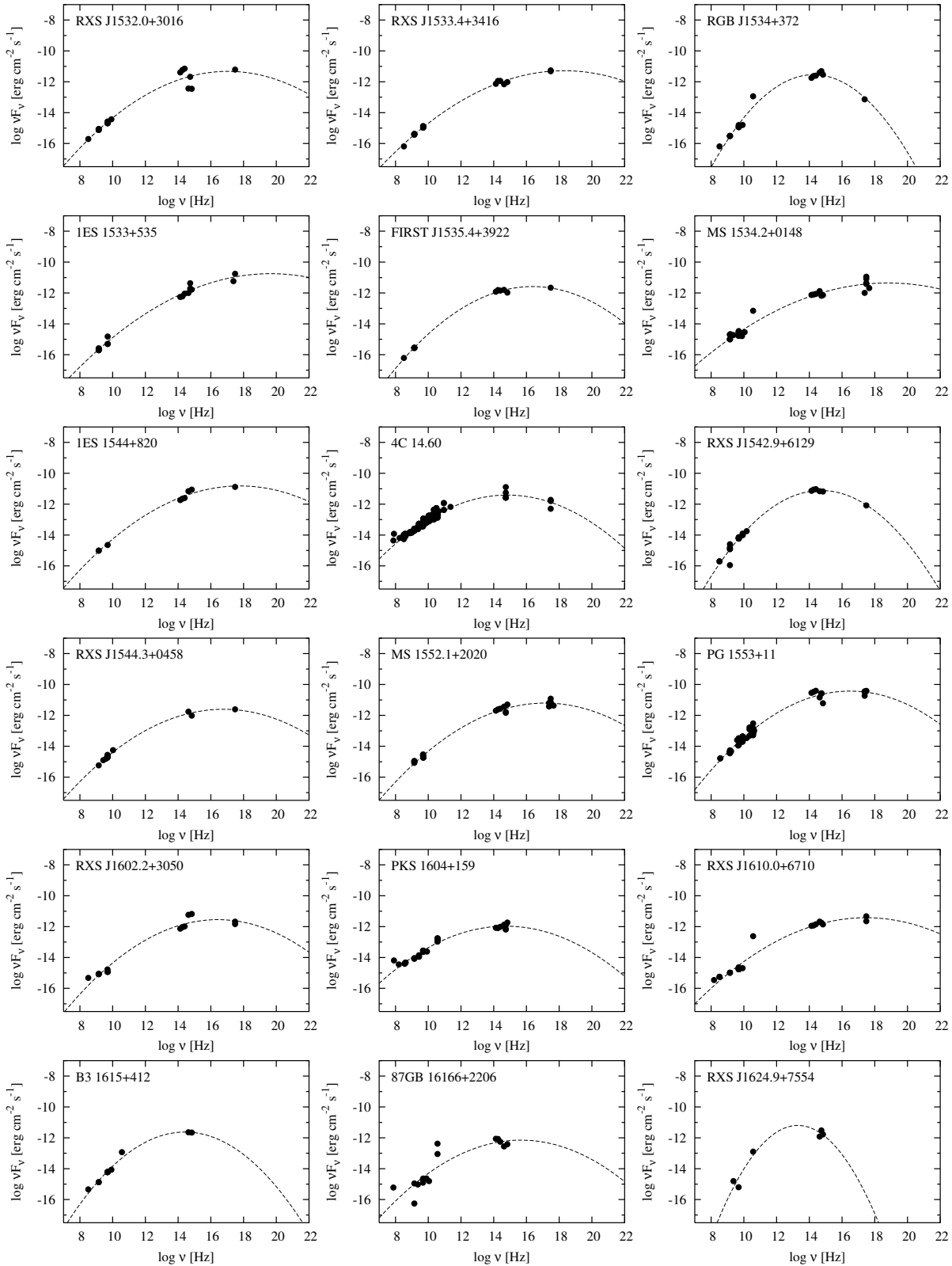


Fig. 13. continued.

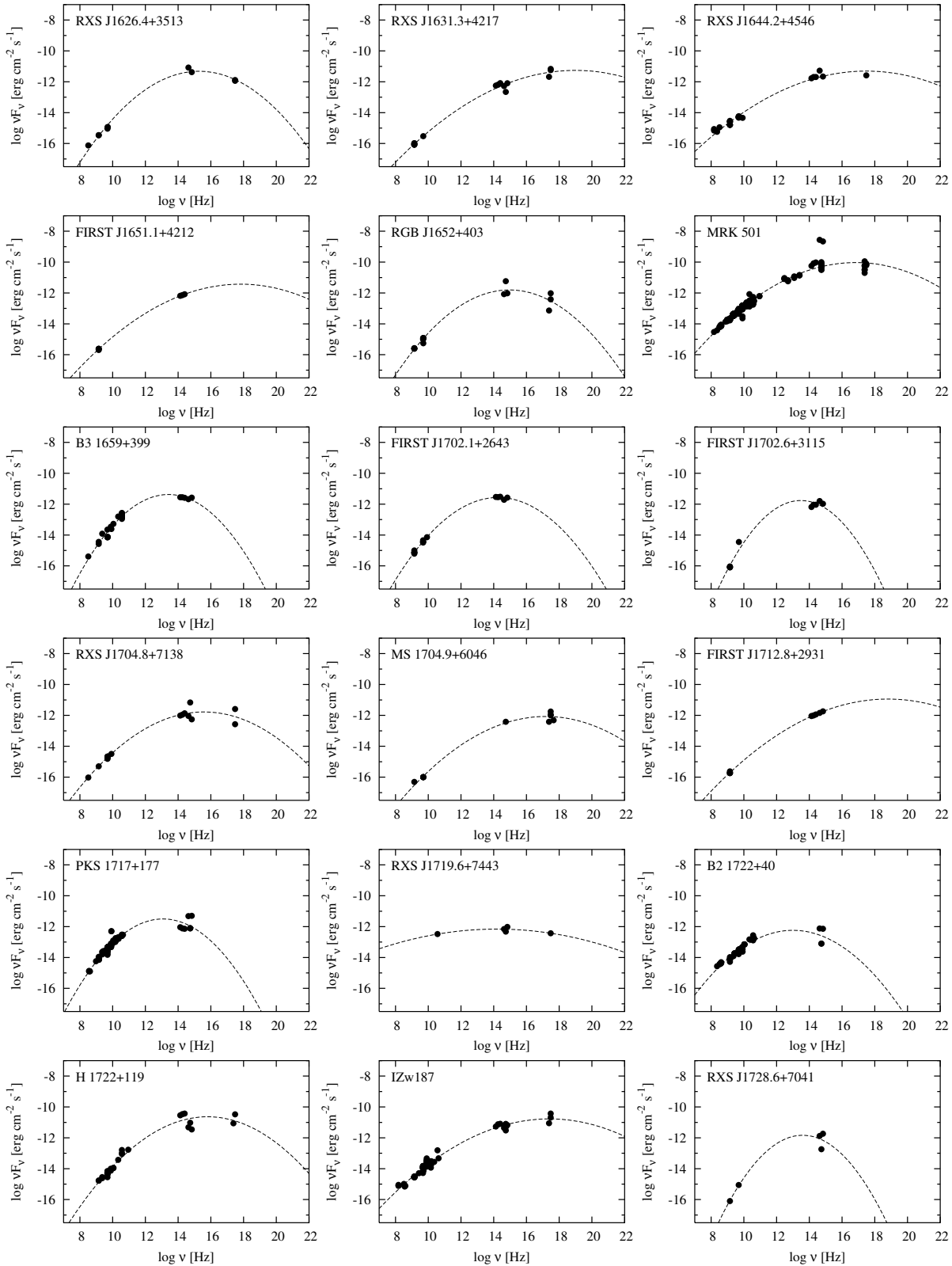


Fig. 13. continued.

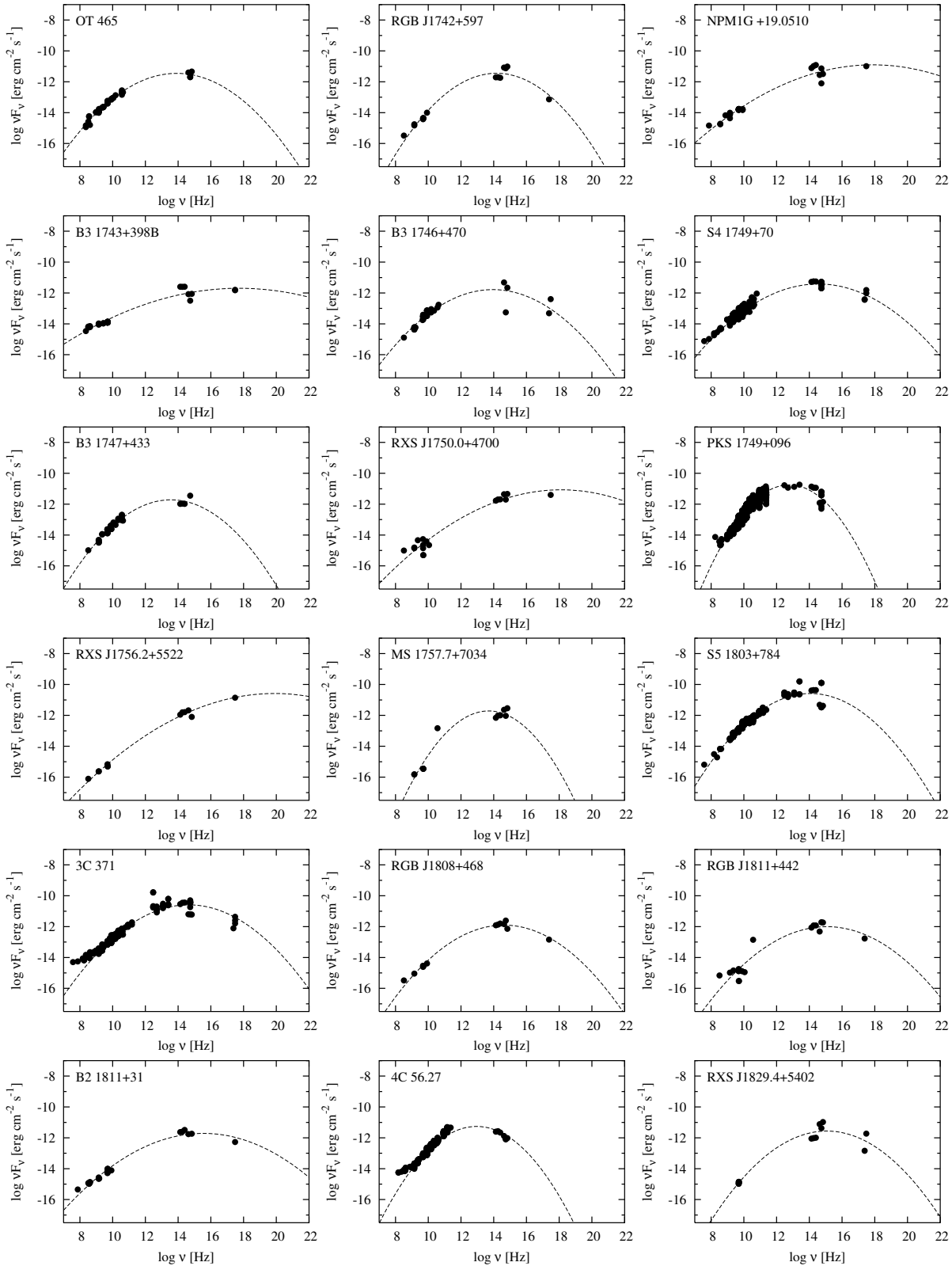


Fig. 13. continued.

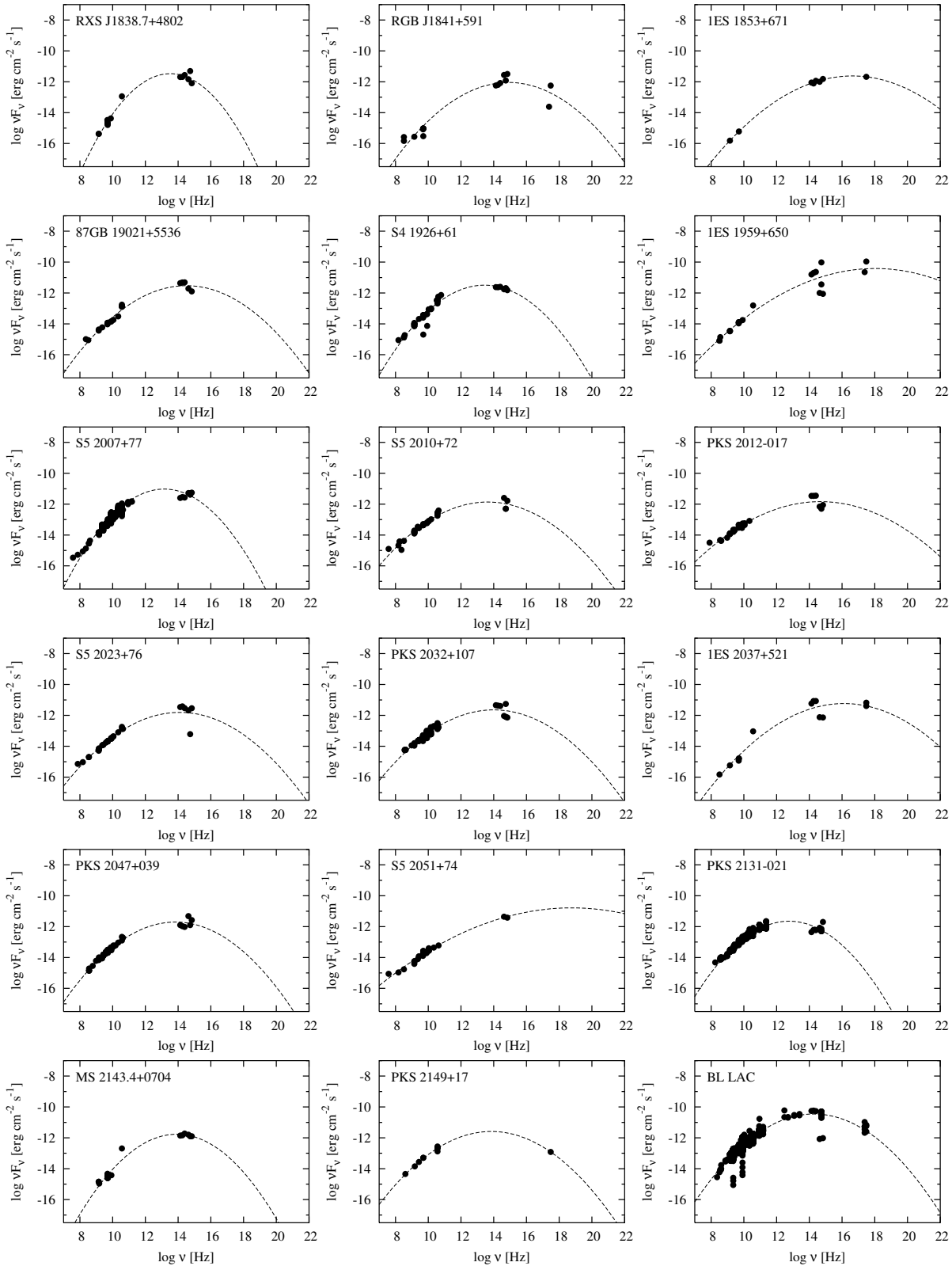


Fig. 13. continued.

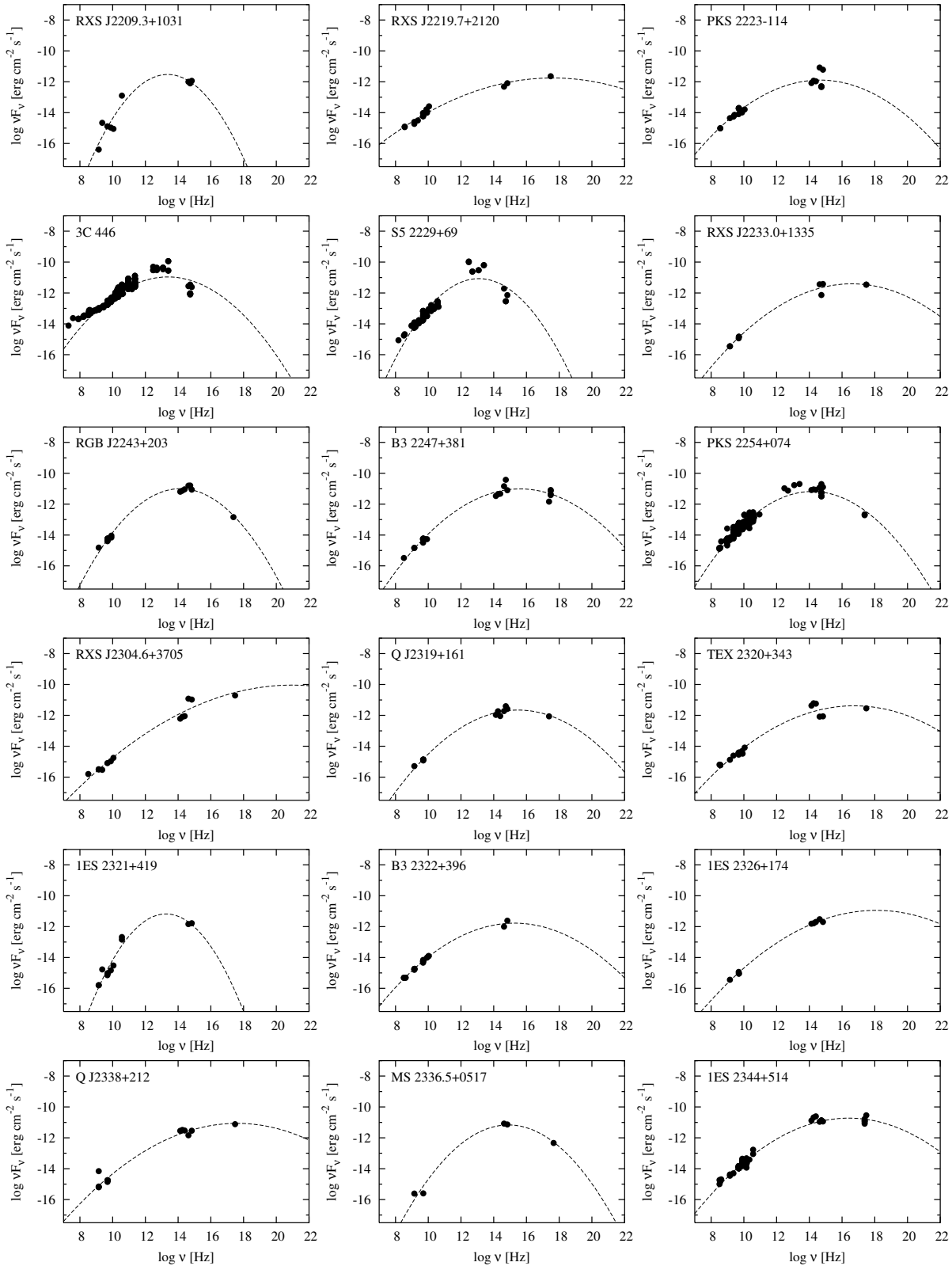


Fig. 13. continued.

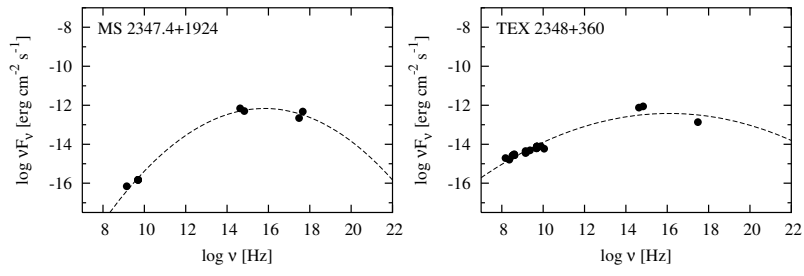


Fig. 13. continued.